CHAPTER

8

CATALYSIS

R. PRINS and D. C. KONINGSBERGER

Laboratory for Inorganic Chemistry and Catalysis
Department of Chemical Engineering
Eindhoven University of Technology
Eindhoven, The Netherlands

8.1. Introduction
8.2. Experimental
8.2.1. Sample Preparation
8.2.2. *In Situ* Cells
8.3. EXAFS of Nonmetallic Catalysts
8.3.1. Homogeneous Catalysts
8.3.2. Transition Metal Compounds
8.3.3. Hydrodesulfurization Catalysts
8.3.4. Adsorption of Bromine and Krypton on Grafoil
8.4. EXAFS of Metal Catalysts
8.4.1. Monometallic Catalysts
8.4.1.1. Structural Properties
8.4.1.2. Catalyst Preparation
8.4.1.3. Gas Adsorption
8.4.1.4. Metal–Support Interaction
8.4.2. Bimetallic Catalysts
8.4.3. White Lines
8.5. Conclusions
References

8.1. INTRODUCTION

Catalysts are materials that are used to improve the activity and/or selectivity of chemical reactions. To make an efficient use of their capacities, and also because they often are expensive, catalysts are used in a diluted or well-dispersed form. Thus in homogeneous catalysis, where catalysts, reactants, and products are dissolved in one and the same phase, the catalyst is a coordination complex

or organometallic compound dissolved in the reaction medium. In heterogeneous catalysis, where the catalyst is in the solid phase while the reactants are in the gaseous or liquid phase, the catalyst may consist of a solid material with a relatively high surface area and large porosity, such as metal sponge (Raney nickel). In this way a large part of the catalytic material can be reached by the gaseous or liquid reactant molecules. In most cases, however, a heterogeneous catalyst consists of a combination of an inert, porous solid material and the catalytically active material. The inert solid functions as a firm support that supplies a large internal surface area on which the active material is deposited in the form of very small particles. Materials like alumina, silica, zeolites, and carbon, with specific surface areas ranging from 1 to 1000 $m^2\ g^{-1}$, are used in large quantities in the petroleum and chemical industries as support materials for catalytically active materials like metals (platinum, rhodium, nickel), oxides (V_2O_5, RuO_2), and sulfides (MoS_2, Co_9S_8). In this way it is possible to reach a very high dispersion of the active material. In most industrial catalysts the dispersion is better than 10% (crystallite size < 15 nm) and in some cases, such as platinum on γ-alumina (denoted as $Pt/\gamma\text{-}Al_2O_3$) used in the catalytic reforming of naphtha to high-octane quality gasoline, the dispersion may even approach 100% (crystallite size ≈ 1 nm). In that case all catalyst atoms are exposed to the gaseous phase and may participate in the catalytic reaction.

It is clear that for spectroscopic studies of such catalysts only techniques can be used in which the radiation can penetrate into and through the support particles and thus reach the interior where the majority of the active material is located. But this also means that the radiation will be able to penetrate the active material.

As a consequence any method, which because of sensitivity reasons has to look at the active material inside the support, is a bulk technique for the active material. This holds for methods like IR, NMR, ESR, Mössbauer, and other spectroscopic techniques, which are used to characterize catalysts on support. The EXAFS technique is also a bulk technique, unless use is made of special, surface-sensitive detection techniques. These techniques are very useful in studies of surfaces of single crystals and films (see Chapter 10) but are not very helpful in the study of material inside the pores of another solid material, like catalysts.

In this chapter the application of the x-ray absorption technique to the study of the structural and electronic state of the catalyst is described. It is shown that by studying the edge and near-edge structure of x-ray absorption spectra information can be obtained about the electronic state of the atoms constituting the catalytic material. This gives valuable information on their oxidation state and sometimes on the symmetry of the site in which the atoms are located. The extended fine structure, on the other hand, gives information about the local structure of the atoms in the catalytic particles, on the number and kind of

neighbor atoms, and their distances. The EXAFS technique is especially useful for the structural study of catalysts since, because of their high dispersion, the catalytically active material on the support of heterogeneous catalysts is present in such tiny little crystallites or particles that other techniques, like x-ray diffraction or electron diffraction, cannot be used. In this respect catalysts have much in common with truly amorphous systems. In case the nature of the chemical state of the active material on the support is unknown or under doubt, the EXAFS method may even clarify which chemical compound is present, as we shall see in Section 8.3.3.

For all heterogeneous catalysts the EXAFS technique opens the possibility to determine the dispersion of the active material and the size and shape of its crystallites. This can be done because one can determine from the EXAFS data the number of nearest-neighbor atoms around a certain atom and also, if present, the coordination numbers of higher coordination shells. These data can be used to test possible models for size and shape of the crystallites. For instance, the nonexistence or broadening of the EXAFS peak in the radial structure function due to atoms in the second-neighbor shell points to very small crystallites or a very amorphous material. The observation of many neighbor shells, on the other hand, proves the presence of well-developed crystals (Section 8.4.1.1).

For many catalysts the EXAFS technique is the only technique with which structural information can be obtained at all. Whenever the dispersion of the active material is high and the size of the crystallites is below 3 nm, the x-ray diffraction lines become too broad to be observable. The standard technique used for such catalysts is the chemisorption method in which the amount of gas is measured that can adsorb on the surface of the active material. From this the size of the active crystallites can be calculated, but in order to do so one has to make an assumption on the stoichiometry of the number of gas molecules that on average adsorb on one surface atom. In practice the chemisorption method works well for metal-on-support catalysts but not for metal oxides and sulfides on support. However, at very high dispersions the method also breaks down for metallic catalysts since in that case nearly all metal atoms are exposed to the gas phase and thus the average number of neighboring metal atoms becomes low. Under these circumstances the number of adsorbed molecules per metal atom may increase dramatically above the commonly assumed values at dispersions of 90% or less (1). This invalidates the chemisorption method, at least for the time being, for the determination of high metal dispersions. The EXAFS technique is extremely useful in studying these high metal dispersions but it is also useful in studying dispersions of metal oxides and sulfides. Some examples will be presented in Sections 8.3.2, 8.3.3, and 8.4.1.

For homogeneous catalysts the EXAFS technique gives information about the local structure (number and kind of surrounding atoms) of the atom or ion in question. In this respect an EXAFS study of homogeneous catalysts is very

similar to that of other complexes in solution, for example, metal enzymes. For a discussion of these biochemical catalysts the reader is referred to Chapter 7.

In this chapter most of the examples of the application of the EXAFS method to heterogeneous and homogeneous catalysis published thus far are discussed. Applications of SEXAFS are not given here but in Chapter 10, since the majority of examples of this technique lie in the field of surface physics. On the other hand, we present the results of measurements of the absorption edges of some catalysts, although a general treatment of the near-edge structure of materials is presented in Chapter 11. We preferred to discuss the measurements of these absorption edges in combination with the EXAFS results.

Before discussing the applications of EXAFS techniques to catalysis in detail, we begin to discuss in Section 8.2 a few general, experimental points that apply to many catalysts. The first is the preparation of the catalyst and the sample to be used in the EXAFS measurement. The second point concerns the need of *in situ* treatment of the catalyst in a special cell to avoid contamination of the catalyst surface by oxygen or any other gas.

8.2. EXPERIMENTAL

8.2.1. Sample Preparation

The high dispersion of the active material on the support of a heterogeneous catalyst makes this material very vulnerable to attack by gaseous compounds. The active material in 1 g of catalyst may easily have a surface area of a few square meters and this amount of surface can, for instance, be covered by all oxygen molecules present as a 1-ppm impurity in 1000 L of inert gas. This means that the contents of an ordinary glovebox, which is filled with an extremely pure inert gas, contains enough oxygen to cover and transform the active material present in a 1-g catalyst sample. Attention should also be paid to the fact that the inside surfaces of gloveboxes continuously give off impurity gases by desorption. From these considerations it becomes obvious that all catalyst handling and treatment should be performed with utmost care. Results obtained on catalysts that have been exposed to air, even for very short periods of time, cannot be trusted to represent the actual catalyst and even results obtained from catalysts handled in good quality gloveboxes should not be taken for granted. Therefore, catalyst preparation has to be performed in *in situ* cells, in which both treatment and measurement can be carried out.

Given the fact that the sample should be treated *in situ* and that, because of the mass absorption coefficients, the sample thickness has to be in the order of a few millimeters, the most appropriate sample form is that of a self-supporting disk (wafer) in open contact to the surrounding atmosphere. Such disks are made

in a similar way as disks used in IR investigations, namely, by pressing the catalyst powder in a die at a pressure high enough for the material to form an adherent entity. The pressure should not be raised too high, otherwise the catalyst particles will be squashed and the active material will no longer be attainable by the gas to be used in the catalyst preparation procedure.

Catalyst preparation of disk-shaped samples is in principal not much different from conventional preparation methods for heterogeneous catalysts. Usually the catalytically active material is brought into the support by impregnating the support material with an aqueous solution containing the cations or anions of the elements that are to be the constituent elements of the active material. For instance, for the preparation of a platinum on alumina catalyst (Pt/Al_2O_3) one may either use a solution of $Pt(NH_3)_4(OH)_2$ or of H_2PtCl_6, while the preparation of a MoS_2/Al_2O_3 catalyst may be started with the impregnation of an alumina sample with a solution of $(NH_4)_6Mo_7O_{24}$. After impregnation the catalyst is dried to remove the water, which otherwise would cause sintering of the active material in subsequent high-temperature treatments. The catalyst now consists of a support with patches of salt distributed over its surface. The dispersion of the salt will depend on the interaction between the salt and the support surface. If the dispersion is high, one may directly proceed with the treatment leading to the final catalyst. For a metal-on-support catalyst, this treatment consists of a reduction with hydrogen, for a metal sulfide-on-support catalyst the treatment consists of reduction and sulfidation with a mixture of, for example, H_2 and H_2S. Such treatments are known as "direct reduction method" and "direct sulfidation method," respectively.

If the dispersion of the salt on the support surface is low, one may want to improve it before starting the final preparation step. It is well known that precursor particles are usually transformed as a whole into product particles and bad precursor dispersions therefore never lead to good catalysts. Improvement of the dispersion of the elements in the salt can, amongst others, be done by oxidation of the salt to metal oxides at elevated temperatures. For instance, both $Pt(NH_3)_4(OH)_2$ and H_2PtCl_6 will be oxidized to PtO_2, while $(NH_4)_6Mo_7O_{24}$ will transform into MoO_3. If the resulting metal oxide has a good interaction with the support, its dispersion may be better than that of the preceding salt. A further advantage of this so-called calcination step is that other elements, which are unwanted in the final catalyst, are blown away as gaseous products. In the examples considered, these gases would be NH_3, NO_x, and H_2O for $Pt(NH_3)_4(OH)_2$ and $(NH_4)_6Mo_7O_{24}$ and HCl and H_2O for H_2PtCl_6. After the calcination step the catalyst is brought into its final active state by reduction, sulfidation, or any other high temperature treatment.

The shaping of the catalyst disk can be done at several points in the catalyst preparation scheme. For instance the pressing of disks can be performed with the support material. In that case the impregnation and drying are carried out

with the disks and the subsequent preparation steps have to be carried out with the disk in its proper position in the *in situ* EXAFS cell. Another possibility is that the disk is pressed after impregnation and drying. Still another possibility is to first prepare a final batch of catalyst powder and then passivate the catalyst material by slowly admitting air (or a mixture of oxygen and inert gas) to the catalyst at room temperature. Care should be taken to do the passivation rather slowly. Otherwise hot spots may arise due to run-away exothermic oxidation of the active material and as a consequence the resulting catalyst may have a bad dispersion due to sintering of the oxidized active material. The carefully passivated catalyst has oxygen adsorbed on the surface of the active material (partial oxidation of this material may also have taken place) and can now be handled in air. Disks can be prepared from this passivated catalytic material, which then can be put in the EXAFS cell to give the final preparation treatment, for example, reduction.

In our laboratory we prefer to prepare the EXAFS samples by the latter route, via passivation of a batch of catalyst powder and preparing disks from the passivated powder. The reason is that in our experience the final treatment step can be performed under much milder conditions after passivation than after calcination or directly after drying. This means that one can take the passivated catalyst material and use it for the preparation of EXAFS disks, as well as for samples to be used in other characterization studies, for instance, hydrogen chemisorption, XPS, IR, and so on. In all these cases one uses the same material and one has to apply only one, not too difficult, final treatment. The chances that in this way the results obtained from the different studies are indeed comparable, are much better than with other methods.

8.2.2. *In Situ* Cells

Compounds that are insensitive to air can be measured in the open air. Pure metals are normally measured as thin foils and salts or other solid materials in pressed disk form. If the material itself is not adherent enough to be pressed into disks, one can admix some polyethylene and press disks at a somewhat elevated temperature (2). Another possibility is to put the material between adhesive tape, between mylar sheets (3), or make a paste that can be put between mylar (4) or aluminium foil (5). Materials that are slightly sensitive to air (bulk solids, which are reasonably protected by their surface-to-volume ratio) may be handled in gloveboxes. Thus Vlaic et al. have mounted samples into a sample holder inside a glovebag filled with dry nitrogen and transferred the sample holder into a cell equipped with mylar windows (4). The cell could be pumped to 10^{-4} Pa and cooled to liquid nitrogen temperature for the duration of the x-ray absorption measurement.

Air sensitive materials, such as metal and metal sulfide catalysts, have to be

measured in *in situ* cells. A few designs for such cells have been described in the literature and all have demonstrated that they are able to give reliable results. The first cell described in the literature was that of Lytle et al. (6) (Fig. 8.1). It consists of two boron nitride parts that are tightly clamped together by screws onto a stainless steel mounting block. The mating surfaces of the boron nitride cell are scrupulously polished, to obtain a good seal. At the junction of the two boron nitride cell parts there is a cavity to hold the catalytic material. The outside surfaces of this cavity, which are in the x-ray path, are machined to a thickness of 1 mm to minimize x-ray absorption by the cell. Different cells can be made with different cavity depths to permit variations in sample thickness. The stainless steel mounting block has connections for inlet and outlet of gases for catalyst treatment and also inlets and outlets for liquid nitrogen to cool the sample for measurements at low temperatures. A heating element surrounds the sample and makes it possible to heat the sample to 773 K. The sample cell and surrounding heating element are housed in a water cooled aluminium block equipped with two mylar windows. The region between cell and aluminium block can be evacuated. By maintaining a gas flow through the sample cell during a measurement and simultaneously evacuating the region surrounding the cell, leaks can only occur outwardly, away from the cell and catalyst. All mono- and bimetallic EXAFS and white line studies of Sinfelt et al. have been performed with this cell (Sections 8.4.1–8.4.3). The sample in Lytle's cell should be in powdered form, so that the gas can flow through it. This has the advantage that

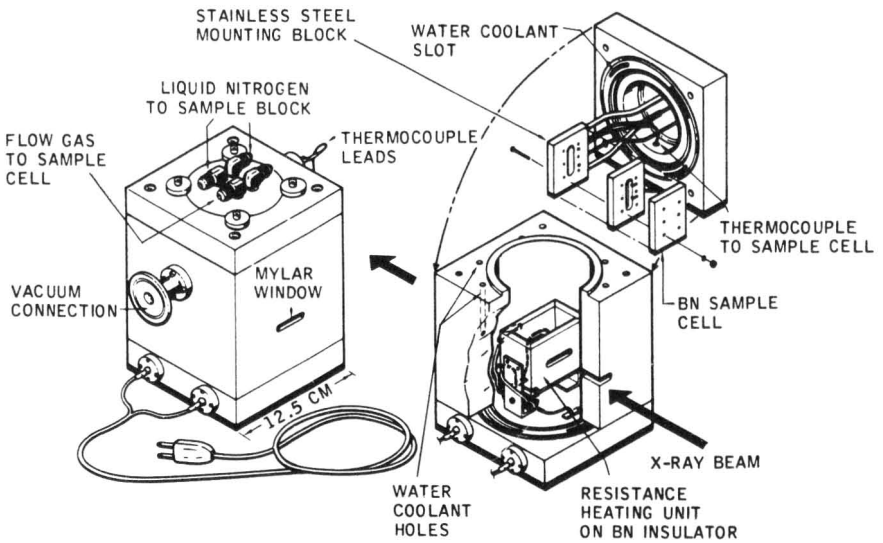

Figure 8.1. *In situ* cell of Lytle et al. (6).

one can use powdered catalytic material without having to press a disk from it. Actually the cell performs as a flow reactor and is therefore very well suited for *in situ* studies. On the other hand, gas absorption studies are difficult to perform, because the cell is not vacuum tight.

Recently, Lytle et al. (7) have added the possibility of fluorescence detection to their cell. They made a window at a right angle to the x-ray beam and followed up on Stern's idea of using an ionization chamber for the detection of the fluorescent x-rays in combination with a $Z - 1$ filter and a Soller slit to suppress secondary fluorescence (8). In this way a good S to N ratio could be obtained even for low catalyst loadings.

A simple cell, resembling cells used in *in situ* IR studies, has been used by Katzer and coworkers (9). It consists of two connecting cylindrical tubes. The double walled vertical cylinder can be filled with liquid nitrogen to cool the frame in which the sample holder is put. The sample consists of a pressed disk in a steel sample holder. The horizontal cylinder is closed at both sides by beryllium windows, which can be removed to put the sample into position at the bottom of the vertical cylinder. Electrical leads for heating the sample and inlets and outlets for gases for catalyst treatment are connected to the horizontal cylinder. The cell is rather easy to construct and to operate, but uses large amounts of liquid nitrogen for cooling, because of poor thermal insulation.

An even simpler cell has been used by Clausen et al. in studies of metal–sulfide hydrodesulfurization catalysts (10). Also, in this case the sample consists of a pressed disk in a stainless steel sample holder. The sample holder can move through a cell which consists of a glass and a metal part (Fig. 8.2). The glass tubular part is equipped with inlets and outlets for gases and can be heated by a mantle furnace. After the treatment of the catalyst the sample in its sample holder is transferred to the brass part of the cell, where it is fixed in position. The upper glass part of the cell is subsequently sealed off. The brass part has x-ray transparent beryllium or mylar windows and can be cooled by partly immersing it into liquid nitrogen. This cell seems very convenient to use. It is easily made, it can be checked for leaks by using a leak detector and, since it is cheap, one can afford to use a cell for each independent experiment. In this way there is no danger of contamination of the next sample, which is especially important when dealing with catalysts that are prepared by sulfiding with H_2S or thiophene. A difficulty might be the gas-tight fastening of the windows to the brass part of the cell.

A high pressure cell for hydrodesulfurization studies has been described by Boudart et al. (11). Convection baffles and cooling jackets allow operation of the catalyst at 523 K and 7.3 MPa while keeping the beryllium windows at room temperature.

In our studies of metal catalysts we have used a cell in which the catalyst

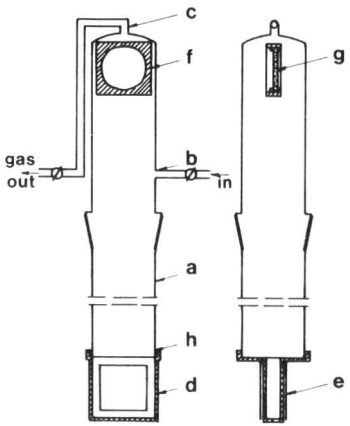

Figure 8.2. Glass sample *in situ* cell used by Clausen et al. (10): (*a*) pyrex glass part, (*b*) inlet of gas, (*c*) outlet of gas, (*d*) brass part, (*e*) beryllium (or Mylar) window, (*f*) stainless steel sample holder, and (*g*) catalyst wafer.

treatment is done with the sample in a position different from that in which it is measured (12) (Fig. 8.3). The pressed-disk-type sample is placed in a sample holder at the bottom of a cylindrical metal tube. Leads for heating and inlets and outlets for cooling the sample with liquid nitrogen run through this inner cylinder. The inner tube and sample holder are positioned in the middle of a wider metal cylinder, which consists of an upper, treatment part and a lower, measuring part. When the inner cylinder is pulled up to a position in which the sample is situated inside the upper part, the upper part is closed off from the lower part by means of a metal flange that is fixed to the bottom of the sample holder. The catalyst is reduced or oxidized in this position by admission of H_2 or O_2 through inlets and outlets through the outer cylinder and by heating the sample holder via the electrical leads through the inner cylinder. The maximum temperature attainable is 773 K. The flange is cooled and this ensures that the lower part of the cell does not come into contact with hot gases. In this way the beryllium windows in the lower part are protected. After catalyst treatment the inner tube with sample is pushed down into the measuring position. During the EXAFS measurement the temperature of the sample can be varied between 77 and 623 K and the cell can be evacuated or filled with gas. In this way the influence of gas adsorption on the catalyst EXAFS spectrum can be easily studied. Recently, we developed a simpler version of this cell in which catalyst treatment (heating) and measurement (cooling) are done with the sample in the same position. The beryllium windows in this cell are water cooled for protection. Because of the strong adsorption of sulfur we use one cell for metal sulfide catalysts and another for other types of catalysts.

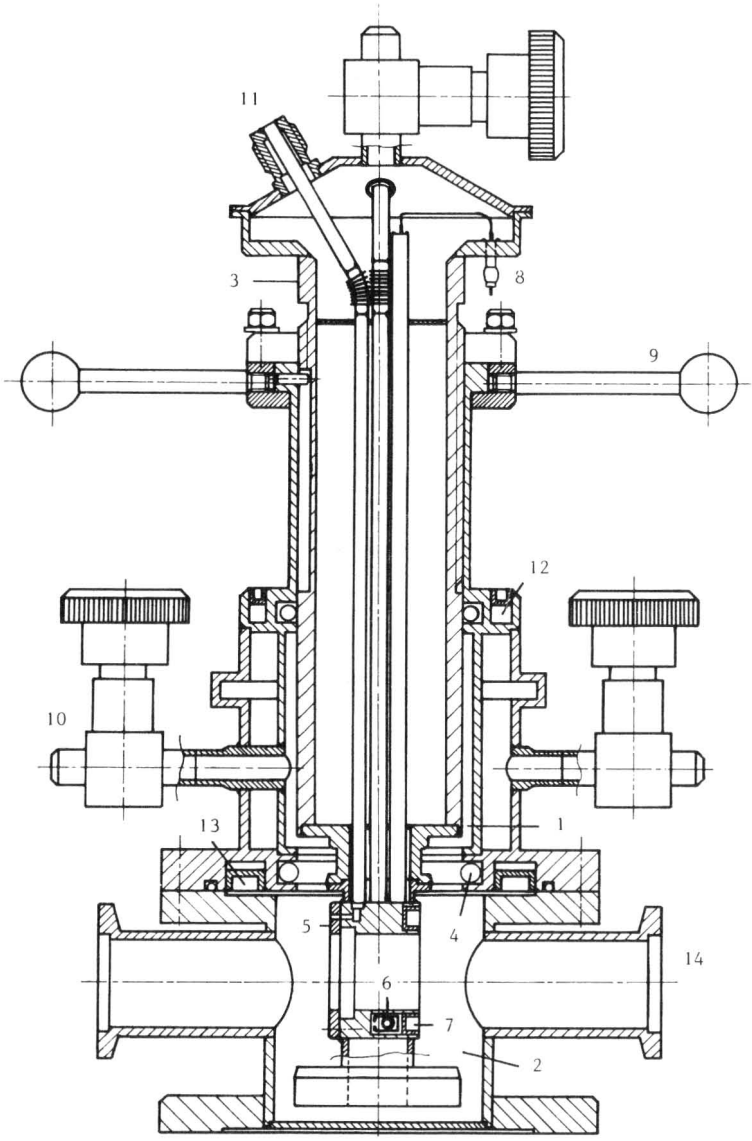

Figure 8.3. Two-compartment cell of Koningsberger and Cook (12): (1) compartment for sample treatment, (2) compartment for measurements, (3) movable inner tube, (4) O-ring seal, (5) sample holder, (6) heater, (7) sample cooling channel (N_2), (8) thermocouple, (9) locking ring, (10) vacuum valve, (11) gas inlet, (12)–(13) cooling channel (H_2O), and (14) beryllium windows.

8.3. EXAFS OF NONMETALLIC CATALYSTS

8.3.1. Homogeneous Catalysts

Up to now only two studies have been reported on real homogeneous catalyst systems, with the catalyst dissolved in solution. All other studies have been concerned with so-called immobilized or heterogenized homogeneous catalysts, in which the actual catalytic complex is attached to a solid support by means of physical or chemical interactions. Immobilization is done to facilitate the separation of catalyst and product in the final solution. In most cases it does not interfere with the chemistry taking place during the catalytic reaction.

In a series of three articles Reed et al. reported transmission EXAFS measurements on Wilkinson's catalyst $RhCl(PPh_3)_3$, the related bromo analogue $RhBr(PPh_3)_3$, and on these catalysts bound to polymers (13–15). These studies are of interest for a better understanding of the structure of the Wilkinson hydrogenation catalyst, especially when supported on polymers. The measurements were performed at SSRL (Stanford University, USA) both on the rhodium and bromine *K*-edges. No details were given of the sample cell used. The data analysis used was more or less equal to the procedure described in Chapter 6. For the chlorine containing catalysts $Rh(Ph_2P-CH_2-CH_2-PPh_2)_2^+$ and $RhCl_3 \cdot nH_2O$ were used as model compounds to obtain the phase and scattering functions for Rh—P and Rh—Cl bonds. For the bromine containing catalysts theoretical phase shifts and amplitudes were used. In the analysis of the rhodium data, contributions from the neighboring halogen and phosphorus atoms were taken into account. The difference between the halogen and phosphorus phase shifts is large enough to distinguish between the contributions of these atoms. In the fitting procedure the sum of the squares of the fit residuals was plotted for several integral values of the number of ligand X and P atoms around rhodium, always assuming a total coordination of four. Since there are two types of phosphorus atoms in the $RhX(PPh_3)_3$ complex, one in trans and two in cis position relative to the halogen atom, also the number of cis and trans phosphorus atoms was varied. In all cases a best fit could be obtained with the sum of the squares of the residuals at least a factor of two better than for the next best fit, indicating that the final best fit represented the actual structure rather well. A small percentage of contribution from other structures could not be ruled out, however. The best fit for the $RhX(PPh_3)_3$ compounds was obtained for $N_X = 1$ and $N_P = 3$. The interatomic distances obtained were in good agreement with x-ray results (Table 8.1).

For the bromine containing compounds, bromine *K*-EXAFS was measured and analyzed. Since the bromine atom has only one nearest neighbor, the

Table 8.1. Interatomic Distances in Wilkinson's Catalysts as Determined by EXAFS and by X-Ray Diffraction

	X = Cl			X = Br			
	I		II	I		I*	II
	X-ray[a]	EXAFS	EXAFS	X-ray[b]	EXAFS	EXAFS	EXAFS
Rh—X	2.376	2.35	2.33	2.587	2.54	2.50	2.50
Rh—P_1	2.214	2.23	2.16	2.176	2.18	2.14	2.16
Rh—P_2	2.326	2.35	2.23		2.31	2.26	2.32

[a]P. B. Hitchcock, M. McPartlin, and R. Mason, *Chem. Commun.*, 1367 (1969); M. J. Bennett and P. B. Donaldson, *Inorg. Chem.*, **16,** 655 (1977).
[b]X-ray results for RhBrP(*o*-vinylphenyl)$_3$. C. Nave and M. R. Truter, *Chem. Commun.*, 1253 (1971).

EXAFS spectrum contains only a single frequency (Fig. 8.4*a*) and hence a single peak in the Fourier transform. In contrast to this, the rhodium atom has three different neighboring atoms and the rhodium EXAFS spectrum thus shows a clear interference between several frequencies, while the Fourier transform contains three peaks (Fig. 8.4*b*).

For $RhX(PPh_3)_3$ bound to a weakly cross-linked phosphinated polystyrene polymer the best fit was obtained for $N_X = 2$ and $N_P = 2$. For Rh(I) compounds such a coordination can only be achieved through dimerization. Apparently the starting compound I (Fig. 8.5) has exchanged one of its triphenylphosphine

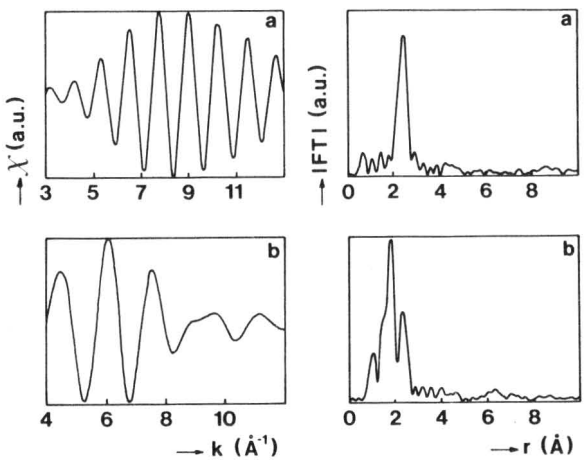

Figure 8.4. (*a*) Bromine *K*-EXAFS and its Fourier transform (magnitude $|FT|$) in $RhBr(PPh_3)_3$. (*b*) Rhodium *K*-EXAFS and its Fourier transform (magnitude $|FT|$) in $RhBr(PPh_3)_3$ (14).

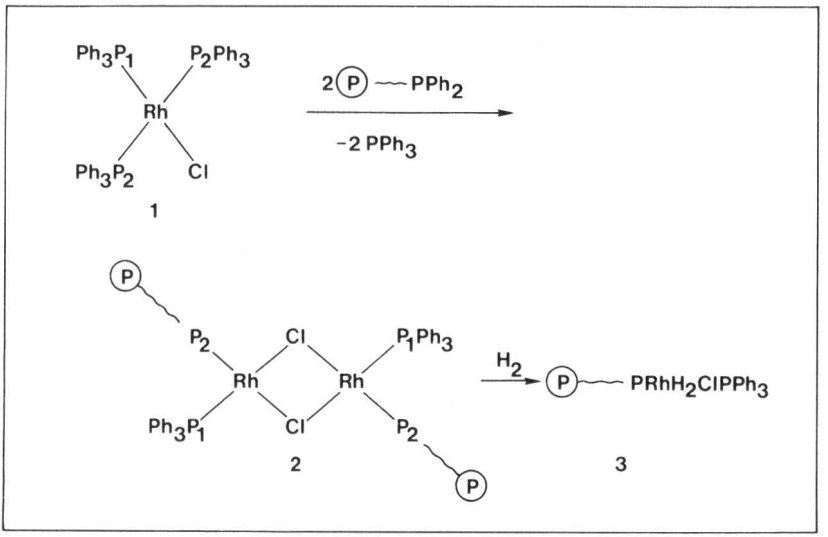

Figure 8.5. Dimerization of $RhCl(PPh_3)_3$, when attached to a derivatized polymer P (13).

ligands for a PPh_2L ligand, where L = cross-linked polystyrene -*p*-C_6H_4-PPH_2, and has subsequently dimerized to compound II (Fig. 8.5). The suggestion that weakly cross-linked polystyrene–divinylbenzene (PS–DVB) copolymers are swellable and mobile and as a consequence promote dimer formation, was proved by measuring the EXAFS spectra of $RhBr(PPh_3)_3$ on 20% cross-linked PS–DVB. In this case the best fit was found for $N_X = 1$ and $N_P = 3$, demonstrating that in this polymer, which is less mobile and has a reduced free volume, dimer formation is substantially reduced. The interatomic distances obtained for the compound I* are presented in Table 8.1.

These structural results are very interesting and encouraging, because they could not have been obtained by x-ray crystallography. Furthermore, they are very relevant for catalysis since the catalyst activity of Wilkinson's catalyst has been found to decrease when bound to polymers. The EXAFS results provide the first real evidence that this is due to dimerization and can be influenced by catalyst (polymer) architecture.

An EXAFS study of real homogeneous catalysts has been reported by Stults et al. (16). In this study model compounds for the rhodium catalyst used in the asymmetric hydrogenation of prochiral alkenes were used. The large interest in this class of catalysts stems from their successful use in the industrial synthesis of L-dopa, a pharmaceutical used in the treatment of Parkinson's disease. Therefore, a structural study of several model complexes was done both in solution

and in the solid state. Rhodium *K*-edge data were obtained at SSRL in the transmission mode. The solution data were obtained by using a glass cell with a 5-cm path length between mylar windows. It must be remarked that such a long path length can only be used when the edge to be studied is far away from the edges of all other atoms present in solution. Rhodium and other 4*d* elements are in a favorable position in this respect. Hydrogen or nitrogen gas could be bubbled through the solution while it was being stirred magnetically. Solutions containing a substrate were added by syringe injection through a septum stopper. An oxygen-free atmosphere was maintained throughout. Data analysis followed the standard procedure. Phases and amplitudes for the bonds between rhodium and phosphous, chlorine, oxygen, and carbon were derived from measurements on $RhCl(PPh_3)_3$, Rh_2O_3, and $(RhL_1L_2)^+ \cdot BF_4^-$, with L_1 = *cis*-bisdiphenylphosphino-ethylene and L_2 = cyclooctadiene. The distances obtained from the EXAFS measurements on compounds in the solid state were in good agreement with crystallographic data and the accuracy of the distances was in the order of 0.02 Å. The solution EXAFS data had a lower accuracy of about 0.07 Å, arising in part from the lack of data above $k = 14$ Å^{-1}, a probable consequence of vibrational damping. A general increase of rhodium-to-neighboring atom bond distances was observed on going from a solid to the corresponding solution. This might reflect relaxation of crystal packing forces, or a failure of the fitting parameters (which were derived from solid-state data) to adequately describe the solution data. In the least squared fit for the unknown compounds only N, R, and σ of the different interatomic distances were varied.

Studies of catalyst and catalyst-substrate intermediates concentrated on the solvated Rh^+ species and on the complex formed with α-acylamino-cinnamic acid. When hydrogen was bubbled through a solution of a $Rh(I)(C_8H_{12})$ complex in methanol, with two monodentate phosphine ligands or one bidentate bisphosphino ligand, two oxygen atoms and two phosphorus atoms were observed in the first coordination shell around rhodium. The two oxygen atoms are most probably from coordinated methanol. Addition of α-acylamino-cinnamic acid to this solution resulted in an EXAFS spectrum that could be analyzed in terms of two different Rh—P distances, a Rh—O, and a Rh—C distance. Apparently a square planar complex is formed with two distinct phosphorus atoms, one trans to the acyl oxygen atom in the substrate and the other trans to the alkene group in the substrate (Fig. 8.6). The Rh—C and Rh—P distances from the *in situ* prepared catalyst–substrate complex agreed favorably with the values for the crystalline compound that was synthesized independently. The Rh—O distance in the *in situ* complex was found to be surprisingly short and may indicate a real difference between the crystalline complex and the active catalytic species in solution. Thus by performing *in situ* EXAFS measurements structural information on two intermediates in the catalytic cycle of asymmetric hydrogenation has been obtained. This structural information is extremely valuable for this

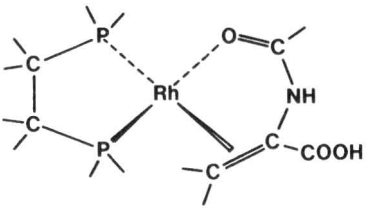

Figure 8.6. Proposed chemical structure for the complex formed when adding α-acylaminocinnamic acid to a solution containing a rhodium(I)diphosphino complex (16).

branch of catalysis, in which the ultimate product of the catalytic reaction is completely determined by the structure of the active catalyst–substrate complex.

Another EXAFS investigation of a real homogeneous catalyst was described by Goulon et al. (17). They studied nickel and cobalt octoate (salts of $C_7H_{15}COOH$) in benzene, before and after addition of triethylaluminium. These Ziegler-type catalysts are used for hydrogenation. Airtight cells with variable optical paths were made of polyethylene or preferably of Delrin and care was taken to fill the cells under perfectly anaerobic conditions. Data analysis was performed by Fourier transformation, corrected for the phase shifts and amplitude factors of the relevant absorber and backscatterer atoms by theoretical estimates, and inverse Fourier transformation. Before reduction the nickel ions were surrounded by six oxygen atoms, at least four of which belong to a monodentate carboxyl group. After addition of triethylaluminium the analysis definitely showed metallic Ni—Ni and Co—Co distances and Ni—X, respectively, Co—X, distances. It was suggested that X might be the carbon atom of an ethyl group attached to a metal atom. Unambiguous fitting of the data with a two-shell model proved impossible. The results suggested that the reduced systems contain small, probably amorphous, metal clusters onto which ethyl groups are attached.

In a short communication Besson et al. showed that the combination of EXAFS with other spectroscopic techniques can be very helpful in the characterization of the structure of complexes (18). They published some results of a combined IR and EXAFS study of the adsorption of osmium carbonyl complexes on the surface of a silica support. When a solution of $Os_3(CO)_{12}$ in CH_2Cl_2 was brought into contact with silica and subsequently dried and heated to 423 K, 2 mol of carbon monoxide evolved and a new IR spectrum was observed. The EXAFS spectrum changed too, but it still contained peaks ascribed to Os—Os bonds, albeit shorter, and no evidence for second neighbor osmium peaks. Therefore, it was concluded that no aggregation to metal particles had occurred and that the cluster framework was still intact.

Similarly, *K*-EXAFS data from unsupported $Rh_2Co_2(CO)_{12}$ and $RhCo_3(CO)_{12}$ complexes and from these complexes on γ-Al_2O_3 (19) revealed that in the catalysts made by impregnation of the dehydrated γ-Al_2O_3 support with an alkane solution of the complexes, the Rh—Rh and Rh—Co bond lengths and coordi-

nation numbers were about the same as those obtained for the powdered unsupported complexes. Putting the clusters on support apparently left the metal skeletons of the clusters intact. After subsequent reduction with H_2 at 673 K the coordination numbers were about the same as those of the corresponding clusters, indicating that the metal skeletons were also retained during reduction. In contrast to these results for the clusters, Rh—Rh and Rh—Co coordination numbers obtained for catalysts prepared by co-impregnation of an aqueous solution of $RhCl_3$ and $CoCl_2$ and subsequent reduction, were much higher and their sums were close to the bulk value of 12. The classic aqueous impregnation method apparently led to rather large bimetallic particles.

Joyner et al. studied the influence of heat treatment of a cobalt–porphyrin catalyst supported on active carbon (2), since such treatments are known to lead to improved oxygen reduction electrocatalysts. Although the data were rather noisy they could see a change in the EXAFS spectrum after a heat treatment of the catalyst. A qualitative analysis of the data indicated that a plausible explanation was that in the cobalt *K*-EXAFS spectrum of the untreated cobalt porphyrine there are four nitrogen atoms in the first shell and eight carbon atoms in the second shell around cobalt, while after heat treatment only the four nitrogen atoms were retained. This might indicate that during heat treatment the carbon bridges connecting the pyrrole fragments in the porphyrin framework are broken.

8.3.2. Transition Metal Compounds

Studies of several transition metal ions on Al_2O_3 catalysts have been performed. Metal ions in and on oxidic supports can occur in different sites and may form various compounds with the support. Nevertheless the resulting EXAFS spectra will be rather similar: The first-shell interatomic distances will be about the same in all oxidic sites and compounds and it is only in the second and third neighbor shells that different environments will show up. This is clearly demonstrated in the copper *K* spectra of CuO and $CuAl_2O_4$ (4,20), where the major difference is found in the range $4 < R < 6$ Å. Since this region is less well developed in catalysts with a high dispersion, it is not so easy to distinguish by means of EXAFS between CuO formation or dissolution of Cu^{2+} into Al_2O_3 catalyst. In combination with other spectroscopic techniques, like x-ray diffraction (XRD), x-ray photoelectron spectroscopy (XPS), ESR, and diffuse reflectance spectroscopy, still worthwhile information could be obtained.

The analysis of the cobalt and nickel *K*-EXAFS spectra of oxidic cobalt and nickel on Al_2O_3 was done by Fourier and inverse Fourier transformation of the first coordination shell, and the log ratio technique was used to determine N and σ for the oxygen ions around Co^{2+} and Ni^{2+} (21). The coordination number of

oxygen ions around Co^{2+} was found to increase from 4 to 5.3 when increasing the cobalt loading of the support. This confirms that at low loading the Co^{2+} ions are in tetrahedral sites in the Al_2O_3, while at high loading bulk Co_3O_4 is formed on the catalyst surface. At all loadings the coordination number for Ni^{2+} was higher than that of Co^{2+}, in line with the higher preference of Ni^{2+} for octahedral sites. Near-edge structures confirmed the EXAFS results, a weak pre-edge peak was observed in all cases, but most intense for Co/Al_2O_3 catalysts. In model compounds the $1s$–$3d$ peak has indeed been observed to be more intense for tetrahedral than for octahedral coordination of the absorbing ion (22) (cf. also Chapter 11, Section 11.5.7).

Studies of Ni^{2+} and Co^{2+} ions in oxides and other materials have also been performed by Tohji et al. (23, 24). The aim of their investigations was to study the preparation of nickel and cobalt metal catalysts via the method of hydrolysis of a mixed solution of a metal alkoxide and ethyl orthosilicate or *n*-propyl orthotitanate. For that reason these investigations will be discussed in Section 8.4.1.2 together with other EXAFS investigations of metal catalyst preparation.

The titanium and vanadium *K*-EXAFS and XANES spectra of vanadium oxide supported on titanium dioxide, which catalyzes the selective oxidation of *o*-xylene to phthalic anhydride, has been studied by Kozlowski et al. (25). Less well-resolved EXAFS spectra of pure rutile and anatase have been measured by Vlaic et al. (26) at Frascati. The study of Kozlowski et al. was performed at Daresbury with a channel cut Si(111) crystal monochromator at low energy of the storagering, thus avoiding contamination of the data by second or third harmonics. Well-resolved spectra were obtained for V_2O_5 and for the anatase and rutile phases of TiO_2. High surface area TiO_2 was found to have the same structure as highly crystalline anatase. However, the correlation of atomic positions was lost beyond distances involving more than three linked TiO_6 octahedra. The monolayer V_2O_5 on TiO_2 catalyst had a different structure than that of crystalline V_2O_5. EXAFS combined with XANES analysis indicated that most probably the V^{5+} ions in the catalyst are surrounded by two terminal oxygen ions at short distance and two bridging oxygen ions at larger distances.

Sato et al. have determined the structure of a molybdenum metathesis catalyst with the aid of a laboratory EXAFS apparatus with a rotating anode x-ray generator and a flat Ge(111) crystal monochromator in fourth-order reflection (27). The catalyst was prepared by impregnation of a solution of $Mo_2(C_3H_5)_4$ on γ-Al_2O_3. After subsequent reduction and oxidation the molybdenum *K*-absorption spectrum was measured. The Fourier transform of χk^3 showed clear peaks due to Mo—O and Mo—Mo distances. Curve fitting was performed by the theoretical method as well as by the empirical method, with Mo and K_2MoO_4 as model compounds. The analysis showed that there are 4–5 oxygen ions at a distance of 2.76 Å and about one molybdenum ion at a distance of 3.2 Å of the absorbing molybdenum ion. This provided proof for the suggestion made in

other studies that the catalyst consists of dimeric molybdenum oxide species on the Al_2O_3 surface.

EXAFS studies of zeolites A and Y ion exchanged with Co^{2+} and Mn^{2+} were published by Morrison et al. (28–30). Both sixfold and fivefold coordination by oxygen atoms at distances equal to that of $M(H_2O)^{2+}$ in solution was observed for hydrated zeolites. For dehydrated zeolites a peak due to backscattering from nearest-neighbor oxygen atoms in the zeolite framework six ring was observed, and also a second peak due to backscattering from silicon, aluminium, and remaining oxygen atoms in the six ring. Some of these results were at variance with crystallographic results. According to Morrison et al. this suggests that there exists static and dynamic disorder of the metal cation complexes in the zeolite and that equivalent crystallographic sites may be occupied by inequivalent cations. The EXAFS technique, being atom specific and insensitive to long-range disorder, may then turn out to be a better probe of the coordination environment of the metal cation. Further studies would be of interest.

Titanium *K*-edge measurements on $TiCl_3$ and $TiCl_2$ Ziegler–Natta catalysts have been published by Reed et al. (3) and by Vlaic et al. (4). The results obtained by these two groups are rather conflicting. One group reports a Ti—Cl distance in $TiCl_3$ of 2.22 Å and the other a distance of 2.46 Å. The reason for this discrepancy is not clear, since both sets of raw data look good. It may be that one of the samples had suffered from oxygen contamination. On the other hand, the most possible product of such a contamination (anatase) has a completely different EXAFS spectrum (25) than observed for the two $TiCl_3$ samples. New measurements under very careful conditions seem to be called for.

8.3.3. Hydrodesulfurization Catalysts

Several studies of Mo, Co—Mo, and Ni—Mo on Al_2O_3 hydrodesulfurization (HDS) catalysts have been published, both of the oxidic precursors to the catalysts and of the sulfidic catalysts themselves (10, 11, 31–36). The samples studied were either commercial catalysts or were prepared by the usual method of impregnation of Al_2O_3 with a solution of $(NH_4)_6Mo_7O_{24}$, followed by drying and calcining. Subsequently $Co(NO_3)_2$ was added by impregnation, drying, and calcining. Clausen et al. (10, 31, 36) and Boudart et al. (11, 32) prepared their EXAFS samples by pressing the catalysts in the oxidic state and sulfiding them *in situ* in the EXAFS cell. Kohatsu et al. (35) and Parham and Merrill (33) first sulfided the catalysts in a reactor and made EXAFS samples with the aid of a glovebag and nitrogen purging. While Parham and Merrill claimed that the molybdenum EXAFS of their samples had not suffered from this handling,

Kohatsu reported that especially nickel could not be kept in the sulfided form in this way.

The most extensive studies of the oxidic precursors to the hydrodesulfurization catalysts have been published by Parham and Merrill (33) and Chiu et al. (34). They not only studied oxidic molybdenum and Co—Mo on Al_2O_3, but also many oxidic molybdenum model compounds. All oxidic catalysts showed one strong peak in the Fourier transform of the molybdenum *K*-EXAFS data at $R = 1.73$ Å. This distance is typical for Mo—O distances in tetrahedrally coordinated molybdenum and for the shorter Mo—O distances observed in octahedrally coordinated molybdenum. For instance in MoO_3 the six Mo—O distances range from 1.67 to 2.34 Å. Other spectroscopic techniques have indeed indicated that after calcination a substantial part of molybdenum is in the tetrahedral form (37). Smaller peaks in the radial structure function were observed at 2.55, 2.86, and 3.5 Å by Chiu et al. (34). They used a new EXAFS data reduction method, analogous to a method used in gas-phase electron diffraction. By smoothing the data to minimize extraneous noise, deconvoluting the spectra to correct for finite energy width of the beam, and correcting for truncation errors they were able to obtain radial distribution curves with substantially lower background noise and high reproducibility of the full width at half-maximum (FWHM) of the major peaks. It is a pity, however, that the authors did not present the uncertainties in the magnitudes of the resulting peaks. Looking at the two figures in which they present "original" data, it is obvious that some of the smaller peaks are very hard to differentiate from noise and this has to result in a rather high uncertainty in the final result. This might explain why the intensities of the small peaks plotted as a function of molybdenum loading on the support were difficult to rationalize. The relative intensity of the peak at 1.73 Å clearly diminished with increasing molybdenum loading, while after addition of cobalt to a catalyst with constant molybdenum loading, increases as well as decreases in the intensity were observed. The decrease in intensity of the main peak in the radial structure function with increasing molybdenum loading was paralleled by an increase in the relative size of a particular peak in the near-edge structure, which was assigned to the $1s \rightarrow 5p$ transition. This increase in intensity in one part of the spectrum and decrease in another part is not uncommon and might be due to the sum rule, which states that the sum over all final states j of the oscillator strengths f_{ij} of all transitions from initial state i to final state j is a constant and equal to the number of electrons in the atom. The observed variations in intensity were correlated by Chiu et al. (34) with increasing distortions of the oxygen atoms surrounding the molybdenum cations with increasing molybdenum loading. A quantification of these distortions could, however, not be made. A quantitative analysis is difficult because of the spread in distance of the first-shell oxygen neighbors of molybdenum. As Eisenberger and Brown have clearly pointed out, the truncation of the EXAFS data below

$k = 3$ Å^{-1} leads to a loss of correlations between $\rho(r)$ and $\rho(r + \Delta r)$ for $\Delta r > 1$ Å (38, 39). This means that in disordered materials such as catalysts the second and further neighbor peaks are easily lost and that even the first neighbor peak may suffer a loss in intensity when the spread in the corresponding metal–ligand distances is large. The work of Chiu et al. shows that this is probably the case for many molybdenum oxides and for molybdenum oxide catalysts. The intensity of the first Mo—O peak of a series of model molybdenum oxide compounds strongly decreased with increasing width. An empirical correction for this effect applied to the catalysts still led to too low a coordination number of 2.5 for catalysts with high molybdenum loadings. Further progress for these catalysts and for materials with similar large degrees of disorder is severely hampered because of these inherent limitations of the EXAFS method at low-k values. Recent studies have indicated, however, that the single scattering formalism might be applicable even in the low-k region (40, 41) and this might be very helpful in future studies of the structure of disordered systems (cf. also Chapter 9, Section 9.3.3).

Analysis of the molybdenum K EXAFS spectra of the sulfided catalysts proved much easier than those of the oxidic catalysts. The Fourier transform of the Mo/Al_2O_3, as well as $Co—Mo/Al_2O_3$ catalyst showed two peaks (Fig. 8.7*a*) at the same distances as in MoS_2 (11, 31–33, 36) and back transformation of the first and second peak showed them to be due to backscattering by sulfur and molybdenum atoms, respectively (31). Whereas Clausen et al. reported a coordination number of six for the coordination of molybdenum by sulfur as in bulk MoS_2 (31, 36), Parham and Merrill reported values that increased with increasing sulfidation temperature but which were always below four (33). Boudart et al. published values below six (32), as well as values equal to six (11). A future reliable determination of the Mo—S coordination number is highly desirable because it may give us information about the size of the MoS_2 crystallite on the support and of the existence of an excess or shortage of sulfur at the edges of these crystallites. For the Mo—Mo coordination number all authors (11, 31–33, 35, 36) found a value substantially below the MoS_2 bulk value of six. This indicates either that some degree of disorder exists outside the first coordination shell or that the MoS_2 crystallites in the catalysts are very small, with a substantial fraction of surface molybdenum atoms. The latter conclusion is in accordance with Mössbauer results (42), which showed that the $Co—Mo/Al_2O_3$ catalyst contains MoS_2-like structures in a highly dispersed state. EXAFS measurements at low temperature might give more quantitative information on the Debye-Waller factor and on the Mo—Mo coordination number. A preliminary measurement at 77 K performed at Cornell High Energy Synchrotron Source CHESS (33) showed very good resolution up to 17.8 Å^{-1} and indicated that the size of the MoS_2 crystallites might not be so small after all, because the second Mo—S and second and third Mo—Mo shells could be

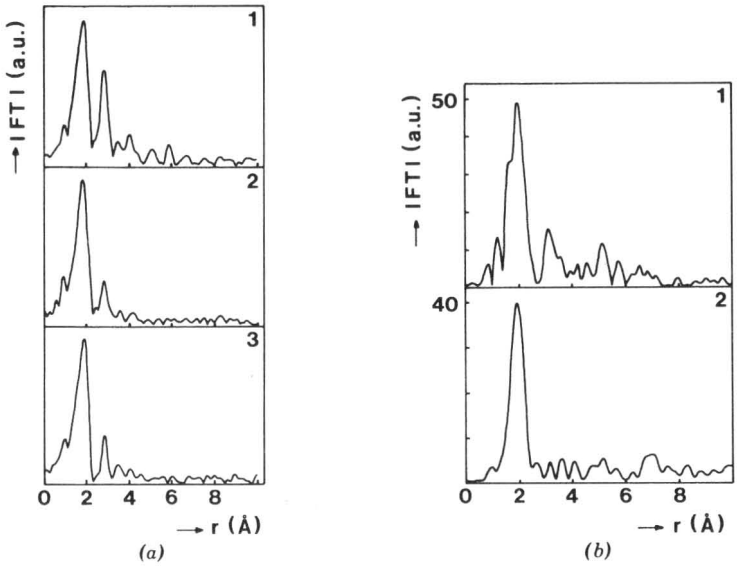

Figure 8.7. (*a*) Magnitude of (k^3) Fourier transform ($|FT|$) of (1) well crystallized MoS_2, (2) sulfided Mo/Al_2O_3, and (3) sulfided $Co\text{-}Mo/Al_2O_3$. (*b*) Magnitude of (k^3) Fourier transform ($|FT|$) of (1) Co_9S_8 and (2) sulfided $Co\text{-}Mo/Al_2O_3$ (31).

observed. In any case the EXAFS results have proven beyond any doubt that in the sulfided Mo/Al_2O_3 catalyst, as well as in the cobalt promoted catalyst, the active material consists of small crystallites of MoS_2. That no molybdenum oxysulfides are present in the sulfided catalysts, as suggested several times in the literature (37), was furthermore proven by the absence of a low-energy 1*s*–4*d* shoulder in the molybdenum *K*-edge.

Boudart et al. have studied the molybdenum *K*-EXAFS as a function of cobalt loading in sulfided $Co-Mo/Al_2O_3$ catalysts (32). By measuring the intensity of the Mo—S peak in the radial structure function they demonstrated that there exists a correlation between the number of sulfur neighbors and the HDS activity as a function of the Co/(Co + Mo) atomic ratio. For N_{Mo-S}, as well as for the activity a vulcano type of curve was obtained. At low Co/(Co + Mo) ratios the cobalt is situated at the edge of the small MoS_2 crystallites, forming the so-called "CoMoS" phase proposed by Topsøe et al. (42). The additional sulfur atoms that go together with this cobalt also function as ligands for the molybdenum edge atoms, thus increasing the average Mo—S coordination number. At large Co/(Co + Mo) ratios most of the cobalt forms separate Co_9S_8 particles, thus depleting cobalt—and thus the extra sulfur—from the "CoMoS" phase.

Comparison of the cobalt *K*-absorption spectra of the $Co-Mo/Al_2O_3$ cata-

lyst with those of several oxidic and sulfidic model compounds demonstrated (Fig. 8.7*b*) that in the sulfidic state the cobalt atoms are surrounded by sulfur (10). This follows from the fact that no 1*s*–4*p* edge peak is present, as in the oxidic catalyst and oxidic model compounds. The Fourier transform of the cobalt *K*-EXAFS showed only one peak, indicating that no well-ordered cobalt sulfide is formed on sulfiding. Admission of oxygen to the sulfided catalyst changed the spectrum drastically and made it comparable to that of oxidic cobalt. This proves that the cobalt atoms are located at the surface of the active phase and supports the "CoMoS" model, which on the basis of cobalt Mössbauer results suggested that the MoS_2 crystallites are decorated with cobalt atoms at substitutional sites at the crystal edges (42).

8.3.4. Adsorption of Bromine and Krypton on Grafoil

Stern and co-workers have made an extensive study of the adsorption of bromine and krypton on graphite (43–45). By using grafoil as a substrate, detailed information could be obtained on the orientation of these adsorbates with respect to the carbon hexagons of the graphitic substrate. Grafoil is an exfoliated conglomerate of small graphite crystallites in a common orientation. About 30% of the total surface area of 22 $m^2\ g^{-1}$ is due to the random oriented crystallites, while the remaining area is on crystallites with basal planes parallel to the macroscopic sheet surface with an rms deviation of 15°. By stacking the grafoil sheets in a cell with their normals horizontal, the angle of the polarization vector with respect to the sheet surface can be varied by rotation of the cell about the vertical axis. When the polarization vector is normal to the planes the contribution of scattering atoms along the normal is emphasized, while with polarization parallel to the plane the scattering of atoms in the plane is enhanced. Thus, by using grafoil as a substrate the relative position of absorbing and scattering atoms can be determined without having to use single crystals.

In the studies of bromine on grafoil (43,44) the factorization of the EXAFS in Br—Br and Br—C contributions was made easy by the fact that the former contribution is important for $k > 6$ Å^{-1}, while the latter is only important for $k < 6$ Å^{-1}. Furthermore, the Br—Br contribution is more important in the parallel spectrum, while the Br—C contribution is more important in the perpendicular orientation (Fig. 8.8). Bromine cannot only be adsorbed at the graphite surface, but it can also be intercalated between graphite layers. The EXAFS spectra of adsorbed bromine at coverages of 0.6 and 0.9 monolayer show a Br—Br scattering that is strongly reduced when the polarization is out of plane, proving that bromine is molecularly adsorbed parallel to the basal planes. In the Fourier transforms only one peak is observed at $R = 2.31$ Å for adsorbed

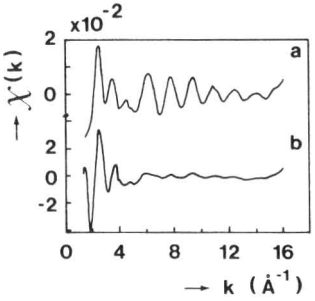

Figure 8.8. EXAFS of bromine adsorbed on graphitic Grafoil sheets with x-ray polarization (*a*) parallel and (*b*) perpendicular to the sheets (44).

bromine. For intercalated bromine $R_{Br-Br} = 2.44$ Å and at 100 K there is an indication for a second bromine atom at 4.1 Å. The Debye-Waller factor for adsorbed bromine is higher than for bromine vapor. For $\Theta = 0.6$ it has the same temperature dependence, but for $\Theta = 0.9$ the temperature dependence is stronger. A full analysis is not possible because the amplitude function of bromine on carbon apparently is different from that of gaseous bromine because of differences in many electron effects. The anisotropy in the EXAFS, as well as in the $1s \rightarrow 4p$ edge line is strongest at low temperature, when the molecules are better aligned.

The analysis of the Br—C EXAFS gave a distance of $R_{Br-C} = 2.9$ Å and a coordination number of $N = 6 \pm 1.5$ at 100 K (with decreasing R with increasing temperature) for the 0.6 and 0.9 monolayer coverages, while $R_{Br-C} = 2.6$ Å and $N = 3$ for the intercalated bromine. The sharp peak in the Fourier transform of the Br—C EXAFS measured at low temperature indicates that each bromine atom in Br_2 is predominantly situated on a specific site. Otherwise, a whole range of Br—C distances would occur and the Br—C EXAFS would be smeared out. Together with the available LEED information Heald and Stern came to the conclusion that the bromine atoms are almost above the centers of adjacent basal plane hexagons. The coordination number of $N = 6$ confirms this. The observed Br—Br distance of 2.31 Å in the adsorption state indicates a stretching of 0.03 Å of the molecule relative to the gas phase, while in the intercalated bromine the interaction with the substrate is so large that the stretching has gone so far (2.44 Å) to almost perfectly match with the distance between the centers of two adjacent hexagons (2.456 Å).

While the orientation of bromine at $\Theta = 0.6$ and 0.9 is nearly identical, at the low coverage of 0.2 and at room temperature the molecule is oriented differently. One atom is bound to a basal plane hexagon with a Br—C distance of 2.4 Å, while the other end of the molecule is free to flop around. The Br—Br distance is the same or slightly less than in the gas phase.

EXAFS measurements of krypton on grafoil were carried out by Bouldin and

Stern in a special aluminium cell with integral windows (45). Measurements were performed at coverages of 0.1, 0.2, and 0.35 monolayer and at 10 and 100 K. In the analysis it was necessary to include the third moment of the radial distribution function of each shell of atoms, because of anharmonicity of the vibrations. For krypton on grafoil μ_0 could be measured directly from the krypton vapor, so that no Fourier filtering or spline fitting was required. Only the $\Theta = 0.35$ sample contained Kr—Kr oscillations. To extract these from the mixture of Kr—Kr and Kr—C oscillations a difference spectrum of $\chi_{\parallel}$ and $\chi_{\perp}$ was made. Since $\chi_{\parallel}$ contained most of the Kr—Kr oscillations it was found that $\chi_{\parallel} - 0.35\ \chi_{\perp}$ was almost free of Kr—C oscillations.

The $\Theta = 0.1$ sample showed more disorder at 10 K and a smaller anisotropy than at higher coverage. This indicates a tighter binding to the substrate for the low coverage sample. The angle between Kr—C and the surface normal is somewhat larger than predicted for the hole or bridge position of krypton above the center of the hexagon or between two carbon atoms. This also suggests that the dominant site for adsorption at higher coverage is the hexagonal hole, but that a fraction of the krypton atoms is adsorbed on tighter bonding defect sites, such as steps and edges.

Distances of $R_{\mathrm{Kr-Kr}} = 4.26$ Å with $N = 1.8 \pm 0.5$ and $R_{\mathrm{Kr-C}} = 3.6$ Å with $N = 7 \pm 2$ were found. The Kr—Kr distance of 4.26 Å is the expected $(\sqrt{3} \times \sqrt{3})30°$ distance, since this is the smallest distance between centers of carbon hexagons that is not excluded by the hard-sphere radii of the krypton atoms. The coordination number of 1.8 is higher than expected on the basis of random distribution and points to ordering.

The bromine and krypton adsorption studies fully demonstrate the power of EXAFS. EXAFS is able to directly characterize the adsorption site and to distinguish changes in adsorption as a function of coverage.

8.4. EXAFS OF METAL CATALYSTS

Most of the EXAFS studies of catalysts have dealt with metal catalysts, in conformity with the fact that metal catalysts are the most widely used catalysts in the industry. Metals of the 5*d* series (osmium, iridium, platinum, gold) and 4*d* series (ruthenium, rhodium, palladium) have been studied most. While the *K*- and L_3-EXAFS of 3*d* and 5*d* metals, respectively, can be studied at most synchrotron storagering facilities, the *K*-EXAFS of 4*d* metals can only be studied when the stored energy of the ring is high (Stanford, Hamburg, Cornell) or when a wiggler magnet is available to shift the critical energy upwards (Stanford, Daresbury, Frascati). In the following the EXAFS on metal catalysts will be discussed under three headings, EXAFS of monometallic catalysts, EXAFS of bimetallic catalysts, and edge structures. The edge structures of metal catalysts

is discussed here instead of in Chapter 11 in order to keep the discussion of metal catalysts together.

8.4.1. Monometallic Catalysts

8.4.1.1. Structural Properties

Via, Sinfelt, and Lytle (46) have studied several Group VIII noble metal catalysts. Their results on monometallic catalysts will be discussed in this section, while the results on bimetallic catalysts and on white lines are presented in Sections 8.4.2 and 8.4.3, respectively. All experiments were performed on catalysts prepared via impregnation of SiO_2 or Al_2O_3 with aqueous solutions of chlorometallic acids, followed by drying and reduction by dihydrogen at 773 K (46,47). After storage in air the catalysts were rereduced in the EXAFS cell with H_2 at 698 K. This cell was described in Section 8.2.2. The analysis of the data followed the standard method. Phases and backscattering amplitudes were determined (46) from the bulk reference compounds Os, Ru, Cu, Ir, Pt, and $Ir_4(CO)_{12}$. The results obtained for the reference compounds demonstrated that the first-shell coordination number N and Debye–Waller factor $\Delta\sigma^2$ can be determined satisfactory, even though these parameters have a high degree of correlation. The uncertainties in these parameters were estimated to be about 20 and 10%, respectively, on an absolute scale. The $\Delta\sigma^2$ data obtained for bulk platinum at elevated temperatures were in excellent agreement with calculations of the mean squares displacements of the platinum atoms about their equilibrium positions by means of a Debye model.

All catalysts studied had a very high degree of metal dispersion ($>70\%$), as determined by chemisorption studies. Nevertheless, the EXAFS spectra of the catalysts were very similar to those of the corresponding bulk metals (Fig. 8.9). Of course the oscillations were smaller because of lower N and higher σ^2 values in the catalysts. A quantitative analysis showed that for these catalysts $7 < N < 10$, while the σ values of the catalysts were about twice as large as those of the bulk metals. The interatomic distances differed by less than 0.01 Å from the corresponding bulk values, except for the Pt/Al_2O_3 catalyst whose R was lowered by 0.017 Å. Since this catalyst had also the lowest N value, the contraction in the interatomic distance may be due to the large fraction of surface atoms in this catalyst.

Measurements over a large temperature range were carried out by Marques et al. for a Pt/SiO_2 catalyst (48). They also improved the data analysis by correcting the EXAFS function of the first coordination shell for the dependence of the phase factor by comparison with platinum foil. In this way the side lobe in the radial distribution function obtained by Fourier transformation of the EXAFS function was removed and the least squares fitting procedure was made

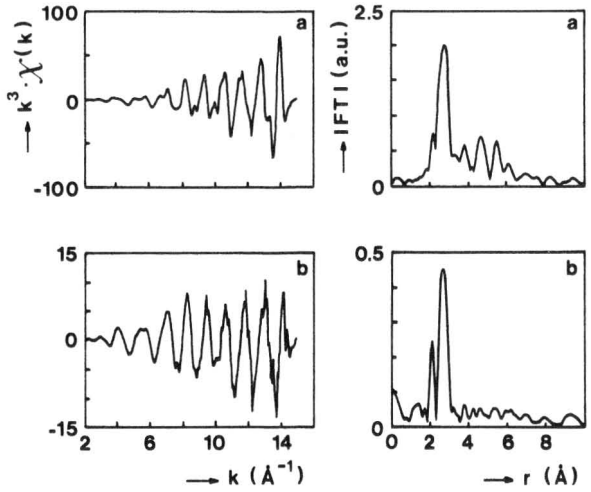

Figure 8.9. EXAFS ($k^3\chi(k)$ and magnitude of (k^3) Fourier transform ($|FT|$) of (*a*) bulk platinum and (*b*) a 1 wt.% Pt/Al_2O_3 catalyst (46).

to converge much easier. The results of the analysis demonstrated large differences between catalyst and platinum foil. R_{Pt-Pt} decreased strongly above 400 K for the catalyst and only slowly for the foil, while the Debye-Waller factor was larger for the catalyst and its temperature dependence was steeper too. The apparent contraction of the interatomic distance in the catalyst with temperature seems to be caused by an inadequate representation of thermal disorder in the simple EXAFS theory.

The EXAFS spectra of the monometallic catalysts (46) were further analyzed by Greegor and Lytle to obtain the coordination numbers (N_2 and N_3) of the second and third shell of neighboring atoms (49). Since N_2 and N_3 are much more sensitive to the size and shape of the metal particles than the coordination number of the first shell (N_1) [for instance $N_2 = 0$ for a one atom thick (111) layer of atoms], the morphology of the metal particles might in principle be determined by comparing measured values with theoretical predictions for different geometrical shape models (spheres, cubes, disks). The method should be most sensitive for small particles below 20 Å and especially for such small particles the normal methods of electron microscopy and x-ray diffraction are not applicable. Furthermore, small particles are also very interesting from a fundamental point of view because they may have a shape and structure different from that of bulk metal particles. On the other hand, the measurement of N_2 and N_3 by EXAFS is difficult because the contribution of the second and third shells to the EXAFS signal becomes very small for small particles. In addition, especially for small particles, one might expect a nonnegligible spread in R_2

and R_3 because of differences in interatomic distances between bulk and surface atoms. As a result the corresponding peaks in the radial distribution function are broad and may even be lost completely when they become too broad, because of the truncation of the data below $k = 3$ Å^{-1} (38, 39). These problems indeed prevented Greegor and Lytle of reaching unambiguous conclusions. They concluded that the osmium particles in Os/SiO_2 were most likely disk shaped, and that the ruthenium, iridium, and copper particles in M/SiO_2 catalysts were most likely spherelike. For the platinum particles, however, all shapes appeared equally possible. The study of Greegor and Lytle (49) shows that the method of determining the morphology of small metal particles by EXAFS, although promising in theory, is very difficult in practice. High quality data measured to high-k values should be available before attempting a quantitative analysis of the second and third shells.

The average coordination number of metal atoms in the small metal particles on the supports of the catalysts is often low, as demonstrated in the studies discussed previously. Therefore, a contraction of the interatomic distances from the bulk metal value is anticipated. Nevertheless, in most cases the contraction was smaller than 0.05 Å and only two studies reported more dramatic contractions. Renouprez and co-workers reported values of 0.13 for Pt/SiO_2 and 0.2 Å for Pt/Y–zeolite (50–52). Their results are based on primary data with low S/N ratios and are in disagreement with the much smaller values observed by others for platinum catalysts. Unambiguous contractions have been reported by Apai et al. for copper and nickel particles made by metal evaporation on amorphous carbon substrates (53). The interatomic metal–metal distance was found to decrease with decreasing coverage of the substrate, as did the threshold energy of the K-edge [similar to shifts observed in x-ray photoemission (54)]. Maximum contractions observed were 0.22 Å for copper and 0.25 Å for nickel. At the lowest metal coverages the interatomic distances approached those of diatomic particles. In agreement with this the EXAFS amplitude decreased with decreasing coverage because of the fact that at low coverage only a small fraction of the metal atoms were present in the form of particles and most atoms were present as isolated atoms.

8.4.1.2. Catalyst Preparation

The EXAFS technique has only been used in a few studies of catalyst preparation up to now and it seems as if one is not fully aware yet of the potential of the technique in this area. Very successful EXAFS studies of the preparation of Ni/SiO_2 and Co/TiO_2 catalysts via hydrolysis of a mixed solution of a metal alkoxide and ethyl orthosilicate or n-propyl orthotitanate were published by Tohji et al. (23, 24). These studies were performed with the aid of a laboratory EXAFS apparatus with a rotating anode x-ray generator. The nickel on SiO_2

(23) and cobalt on TiO_2 (24) catalysts were made by dissolving the appropriate metal nitrates in ethylene glycol, followed by addition of ethyl orthosilicate, filtering, and washing of the resulting gel, followed by drying, calcination, and reduction by hydrogen. Nickel or cobalt *K*-EXAFS spectra were taken after each preparation step. The Fourier transform of the nickel *K*-EXAFS spectrum of the gel formed by addition of ethyl orthosilicate to the solution of nickel nitrate in ethylene glycol showed one peak at $R = 2.05$ Å belonging to the $Ni^{2+}-O^{2-}$ distance (23). Although the ^1H NMR spectrum indicated that the $Ni[OSi(OEt)_3]_2$ species had been formed, the silicon atoms in the second shell could not be seen with EXAFS. After drying at 383 K a second peak at $R = 3.30$ Å showed up, however. Inverse Fourier transformation and comparison with a calculated transform showed good agreement when silicon was taken as scatterer, but no agreement when nickel was taken as scatterer atom. The reason that the second silicon shell is not seen in the gel is, according to the authors, due to the uncertainty in the position of the silicon atom. In the gel rotation of the O—Si group around the Ni—O bond is possible, while in the dried gel the position of the silicon atoms relative to the nickel atoms is fixed. It is hard to visualize, however, how a rotation without a change in bond length can make the second shell disappear. Another explanation might therefore be that in the gel there are oxygen atoms of water molecules as well as silicon atoms at a distance of about 3.3 Å from the Ni^{2+} ion. Since the phases of oxygen and silicon differ by nearly π radians their contributions to the EXAFS signal will cancel each other. Drying removes the water molecules and makes the Ni—Si contribution observable.

Calcination of the dried sample led to a spectrum resembling that of NiO, with Ni—O and Ni—Ni peaks in the Fourier transform. Differences in the relative magnitudes of these peaks compared to NiO were attributed to a small contribution of Ni—O—Si species. This and additional IR and electron microscopy results led to the conclusion that the NiO particles formed in the alkoxide method were smaller than 20 Å and had silicate groups at their surface. After reduction the Fourier transform of the EXAFS spectrum indicated that metallic nickel particles had been formed. The analysis of the EXAFS spectra of nickel catalysts prepared via the classic impregnation route demonstrated that much larger NiO and nickel particles were formed in this method than in the alkoxide method.

In the analogous preparation of a cobalt on TiO_2 catalyst no Co—O—Ti bond formation was observed after addition of $Ti(OC_3H_7)_4$ to a solution of cobalt nitrate in ethylene glycol and drying of the resulting gel at 383 K (24). Apparently the Co—O—Ti structure is not as rigid as the M—O—Si structure. After calcination at 723 K the Fourier transform showed four peaks at the same positions as those of Co_3O_4, but with magnitudes decreasing rapidly with distance. Thus after calcination at 723 K small Co_3O_4 particles were formed, of about 8-Å diameter. Calcination at 973 K, however, led to the formation of $CoTiO_3$ (24).

Lagarde et al. have published EXAFS data on Pt/Al_2O_3 catalysts during different stages of preparation (55, 56). They observed that after impregnation of the support with H_2PtCl_6 or H_2PtBr_6, followed by drying, the EXAFS was almost equal to that of chloro- or bromoplatinic acid in solution. After calcination at 803 K the EXAFS had changed and analysis showed that most of the chlorine and probably all of the bromine had been removed from the first coordination shell of platinum. Apparently, the PtX_6^{2-} complex had been transformed in PtO_2. On the other hand, calcination at 973 K led to the appearance of the EXAFS of metallic platinum. This is in agreement with the known thermodynamic instability of platinum oxides above 873 K. After reduction with H_2 at 753 K a Pt—Pt peak was observed in the Fourier transform with $N = 6$. The Debye-Waller factor quoted was, however, hardly different from that of platinum foil, which is very surprising for small metal particles. Lagarde et al. also compared second- and third-neighbor shells with shape models for metal particles. However, because of very poor signal to noise, their conclusions based on these higher-shell peaks seem highly premature.

Further platinum L_3-EXAFS studies were performed on bimetallic Pt—Re and Pt—Rh on Al_2O_3 catalysts (57, 58). Because of the presence of the rhenium L_2-edge at about 400 eV above the platinum L_3-edge, the platinum EXAFS data for the $Pt—Re/Al_2O_3$ catalyst were restricted to $k < 9$ Å^{-1}. The addition of a second metal salt (NH_4ReO_4 or $RhCl_3$) had a strong influence on the state of the Pt^{4+} ions in the catalyst. Whereas in the monometallic catalyst the $PtCl_6^{2-}$ complex stayed intact during drying at 383 K, the first neighbor shell of Pt^{4+} in the dried bimetallic catalyst consisted of both chlorine and oxygen ions. For the dried Pt—Re catalyst $N_{Pt-Cl} \approx 2$ and for the dried Pt—Rh catalyst $N_{Pt-Cl} \approx 4$. After calcination in air at 803 K the bimetallic catalysts, as well as the monometallic catalyst, showed about 2 Cl ions in the first shell. Surprisingly, in all cases (dried and calcined) the total number of atoms in the first shell around the Pt^{4+} ions was found to be about eight. All these results are intriguing, but require many more experiments before a definite conclusion can be drawn. For instance, the changes in the first coordination sphere of Pt^{4+} by the addition of the second metal salt may be simply due to changes in the Pt^{4+} and Cl^- concentration or to changes in the pH. It is obvious that further studies along the lines described by Lagarde et al. (57, 58) might provide very valuable information on the state of the metal ions on the catalyst support after various catalyst treatment steps.

8.4.1.3. Gas Adsorption

Admission of oxygen to metal catalysts has been studied by several groups. Joyner reported only one peak in the Fourier transform of the EXAFS function of Pt/SiO_2 and Pt/Al_2O_3 catalysts oxidized at 773 K and assigned it to a Pt—O distance (59). The fact that no second- or third-shell distances were observed

was explained as being due to the amorphous character of the platinum oxide particles.

Nandi et al. exposed Pt/SiO_2 (60) and Pd/SiO_2 (61) catalysts to air and demonstrated that for catalysts with a low dispersion the Fourier transform of the platinum L_3, respectively, palladium *K*-EXAFS consists of a metal–metal peak, while the highly dispersed catalysts show a metal–oxygen peak. When the dispersion was about 60%, exposure to air resulted in crystalline Pt_3O_4 or PdO particles with small metallic cores, while for 80% dispersion the particles were fully oxidized. These results are in good agreement with temperature programmed oxidation and reduction studies of well-dispersed metal catalysts, which showed that oxidation of metal particles is diffusion limited (62). As a consequence small metal particles may be totally oxidized already at room temperature, while large particles can only be completely oxidized at elevated temperatures. Exposure of large particles to air room temperature only leads to oxidation of the outer layers.

Fukushima et al. have published results (63) on the adsorption of dioxygen on two reduced Pt/Al_2O_3 catalysts with H/M chemisorption values of 0.47 and 1.14 (mean particle size 26 and < 10 Å, respectively). EXAFS spectra measured at 90 K in an *in situ* cell before and after gas admission showed dramatic influences of catalyst dispersion and of the way in which dioxygen was admitted. Thus admission of 10-Torr O_2 at 77 K to the reduced Pt/Al_2O_3 catalyst with $H/M = 1.14$ changed the Fourier transform significantly. The metallic Pt—Pt peak decreased in intensity by about 30% and shifted 0.25 Å to a shorter distance and a new Pt—O peak appeared at 2.0 Å. Slow warming of the sample to room temperature changed the Fourier transform further. The Pt—Pt peak disappeared and only Pt—O and Pt—Pt peaks of platinum oxide could be observed. This demonstrated that while O_2 admission at 77 K leads to chemisorption and only to a slight oxidation and disruption of the platinum particles, warming up to 300 K under dioxygen causes complete oxidation of the small (< 10 Å) particles. The same treatment (O_2 admission at 77 K and warming up to 300 K during 45 min) did not disrupt the 26-Å platinum particles of the catalyst with $H/M = 0.47$. The EXAFS spectrum was almost the same as that after reduction and the Pt—Pt peak in the Fourier transform underwent $< 10\%$ reduction in intensity. On the other hand, direct room temperature admission of O_2 to this catalyst with $H/M = 0.47$ induced substantial oxidation and disruption. The metallic Pt—Pt peak was reduced by 50% and shifted by -0.2 Å and new Pt—O and Pt—Pt peaks of PtO_2 appeared (Fig. 8.10). These results of Fukushima et al. are in perfect accordance with the results obtained by Nandi et al. and demonstrate that oxygen chemisorption is not restricted to the outermost layer of metal atoms, but leads to oxidation of a skin of several atom layers.

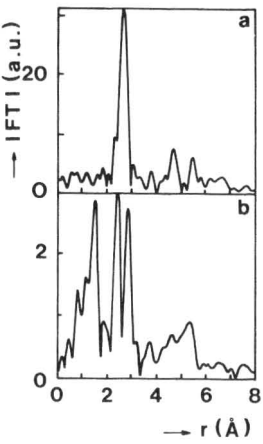

Figure 8.10. Magnitude of (k^3) Fourier transform of (*a*) a reduced Pt/Al_2O_3 catalyst (H/Pt = 0.47, *d* = 26 Å) and (*b*) Pt/Al_2O_3 after admission of 10 Torr O_2 at 298 K (63).

Oxygen adsorption studies on ruthenium catalysts by Lytle et al. (64) confirm the results for platinum and palladium. Thus after dioxygen admission at 298 K to a Ru/SiO_2 catalyst the Fourier transform of the ruthenium EXAFS showed a peak at the metal Ru—Ru distance, as well as a Ru—O peak, demonstrating that at 298 K chemisorption had taken place. After exposure of the catalyst to O_2 at 673 K the metal Ru—Ru peak had disappeared and two new peaks due to Ru—O and Ru—Ru distances like in RuO_2 appeared. Thus at 673 K full oxidation took place. Similar results have been published by Cox (65).

Fukushima et al. also admitted carbon monoxide to their Pt/Al_2O_3 samples and observed new peaks in the Fourier transform around 1.5 and 3.6 Å for the best dispersed catalyst [due to Pt—C and Pt—(C)—O distances, probably] and a shift of −0.12 Å for the metallic Pt—Pt peak (63). The fact that the EXAFS spectrum of the less well dispersed catalyst did not change on admission of carbon monoxide—similar to its invariableness to dioxygen admission—was ascribed to much larger metal particle size. For platinum particles that have 50% of their atoms at the surface one calculates that on average $N(Pt—Pt) = (12 + 9)/2 = 10.5$, while $N(Pt—O) = 3/2 = 1.5$ for chemisorption of oxygen atoms in hollow sites on the metal surface. Together with the much lower backscattering amplitude for oxygen this leads to very low ratios of Pt—O and Pt—Pt peaks in the Fourier transform.

The substantial decrease in Pt—Pt distance when absorbing dioxygen or carbon monoxide was claimed to be real. Renouprez has observed a similar effect upon dioxygen adsorption on Pt/Y-zeolite and Pt/SiO_2 catalysts (50–52). As noted by Burwell [cf. discussion at the end of Fukushima's article (63)] this shortening is in disagreement with x-ray diffraction results, which

showed that the lattice constants of passivated platinum and palladium catalysts differed by <0.01 Å from that of well-reduced catalysts. We therefore suggest that the shift of the Pt—Pt peak upon gas adsorption is not real but is caused by an interference between (nearly) coinciding Pt—Pt and Pt—O peaks. A thorough analysis of the imaginary part of the Fourier transform may solve this problem.

The influence of adsorbed gases on the topology of the rhodium particles on Al_2O_3 has been studied by van't Blik et al. (66–68). They demonstrated that the Rh-Rh oscillation in the rhodium K-EXAFS vanished when carbon monoxide was adsorbed on a highly dispersed and well-reduced Rh/Al_2O_3 catalyst. This proved that disruption of the small rhodium particles had taken place. The Fourier transform of the resulting EXAFS spectrum showed three peaks due to Rh—C, Rh—O (oxygen from the carbonyl group) and Rh—O (from the support) distances. With the aid of $[Rh(CO)_2Cl]_2$ and Rh_2O_3 as reference compounds a full analysis of the data could be made showing that after carbon monoxide adsorption each rhodium atom was surrounded by two carbon monoxide molecules and three oxygen ions from the support (Fig. 8.11). From complementary ESR, XPS, and IR studies it was concluded that the oxidation state of rhodium was 1+. Thus $Rh(CO)_2^+$ species had been formed that were attached to three oxygen ions of the support. This EXAFS study proved that a former suggestion put forward on the basis of IR experiments on carbon monoxide adsorbed on Rh/Al_2O_3 catalysts was true and settled the question whether fully reduced rhodium particles existed at all before carbon monoxide adsorption. The $Rh(CO)_2^+$ species could be transformed into rhodium particles by desorption at 573 K (68). The EXAFS spectrum showed the reappearance of slightly sintered rhodium particles. Heating a Rh/Al_2O_3 catalyst to 523 K under flowing carbon monoxide resulted in a very complicated EXAFS spectrum, but nevertheless it could be established that during the Boudouard reaction ($2\ CO \rightarrow CO_2 + C$) the Rh—Rh bonds were disrupted. On the other hand, heating of a Rh/Al_2O_3 catalyst under flowing synthesis gas ($CO + H_2$) kept the catalyst in the metallic state, although some sintering occurred as judged from the value of N.

The disruption of the rhodium particles by carbon monoxide proved to be dependent on the metal particle size. Whereas an extremely well dispersed 0.6 wt.% Rh/Al_2O_3 catalyst with $N_{Rh-Rh} = 3.7$ showed no Rh—Rh EXAFS contribution after adsorption of carbon monoxide, the EXAFS of a 1 wt.% Rh/Al_2O_3 catalyst ($N_{Rh-Rh} = 5.9$) and of two Rh/TiO_2 catalysts with rhodium loadings of 0.5 and 1 wt.% ($N_{Rh-Rh} = 4.4$ and 5.9, respectively) not only showed the presence of $Rh(CO)_2^+$ species after carbon monoxide adsorption, but also still the presence of some Rh—Rh bonds (68–70). Apparently the larger particles present in these catalysts cannot be broken up by carbon monoxide adsorption, because the heat of adsorption of carbon monoxide is only sufficient to break a limited number of Rh—Rh bonds (71). The support does not influence

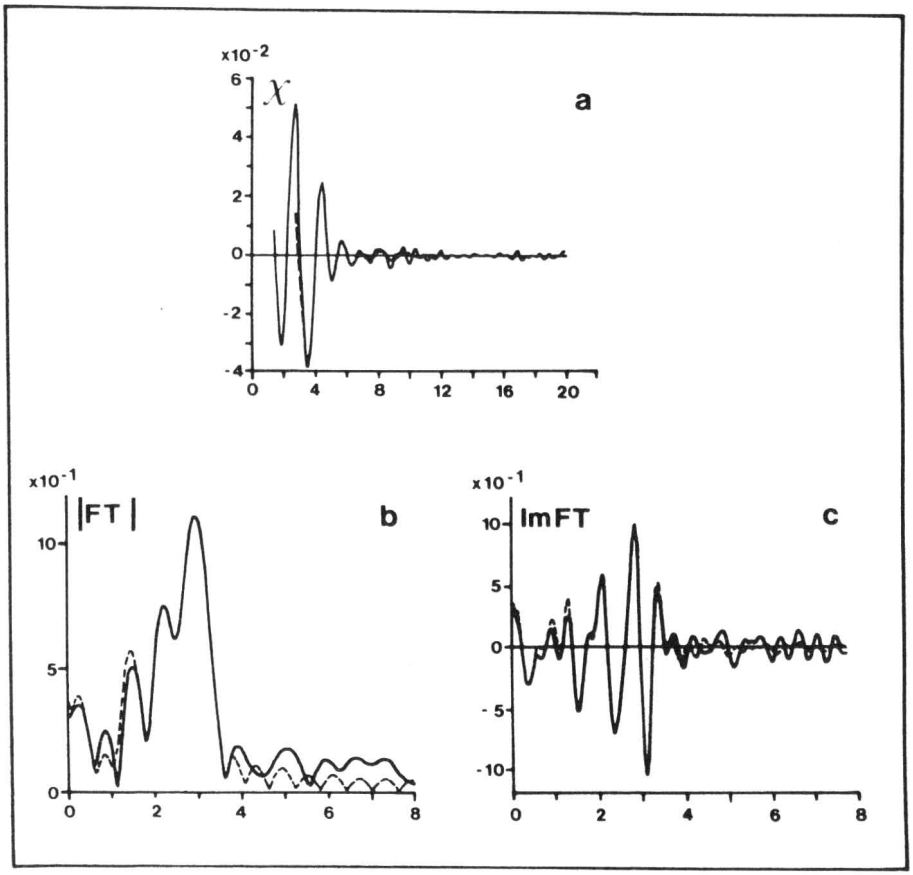

Figure 8.11. (*a*) Rhodium *K*-EXAFS of a Rh(0.57 wt.%)/γ-Al_2O_3 catalyst after CO admission at room temperature, (*b*) and (*c*) magnitude ($|FT|$) and imaginary part, respectively, of the (k^3) Fourier transform (corrected for the Rh—O phase shift). The solid lines represent the data and the dotted lines represent the calculated Rh—(C)—O + R—O EXAFS (67).

the structure of the $Rh(CO)_2^+$ species formed during carbon monoxide adsorption. The distance between the rhodium cation and the O^{2-} anions of the support is the same for γ-Al_2O_3 and TiO_2 supported systems (2.12 Å), and also the number of Rh^+—O^{2-} bonds is equal to three for both supports (67, 69, 70).

8.4.1.4. Metal–Support Interaction

A very important issue in catalysis is the interaction between the catalytically active phase and support, since it is this interaction that prevents catalyst par-

ticles from sintering. For metal catalysts several models have been proposed to describe the structure of the metal–support interface. Most models assume the presence of metal cations at the interface in order to be able to invoke strong coulombic forces instead of weak van der Waals forces for explaining the metal–support interaction. Thus cations of the metal proper or intentionally added cations have been suggested to be present in the metal–support interface and to function as an anchor for the adhering metal particle (71). For some catalysts even complete interfacial metal oxide layers have been proposed (72). A few EXAFS studies have addressed the problem of the metal-support interface and have claimed to have observed metal cation to oxygen anion distances at the interface. Thus Lytle et al. attributed a peak in the Fourier transform of the ruthenium *K*-EXAFS of Ru/SiO_2 to such a Ru—O bond (64). Lagarde et al. assigned a Pt—O bond in a Pt/Al_2O_3 catalyst to platinum cations at the interface (55), and Bassi et al. claimed that peaks in the Fourier transform of the gold L_3-EXAFS of Au/MgO catalysts were due to Au—O bonds in the Au—MgO interface (73, 74). In these studies the metal-to-oxygen distances were equal to those expected for $M^{n+}—O^{2-}$ distances. Although the catalysts were said to be well reduced, in none of the mentioned studies was clear evidence presented as proof that the metal cations were actually present at the metal–support interface, instead of present in special, difficult to reduce sites on the support surface. Studies of Rh/Al_2O_3 (75) and Pt/Al_2O_3 (76) catalysts by Koningsberger et al. have shown that in these catalysts $Rh^{3+}—O^{2-}$ and $Pt^{4+}—O^{2-}$ distances were only observed in the catalysts had not been completely reduced. A 2.4 wt% Rh/Al_2O_3 catalyst, which had been calcined at 623 K and reduced at 473 K, showed the presence of a 2.05 Å $Rh^{3+}—O^{2-}$ bond that disappeared after reduction at 673 K (Fig. 8.12).

In an extended analysis of well reduced and highly dispersed Rh/Al_2O_3 catalysts (with H/Rh ranging from 1.2 to 1.7) van Zon et al. again found no evidence for $Rh^{3+}—O^{2-}$ distances, but they did find a peak at 2.7 Å in the Fourier transform of the rhodium *K*-EXAFS belonging to a rhodium atom to oxygen anion ($Rh^0—O^{2-}$) distance (77, 78). To be able to distinguish this $Rh^0—O^{2-}$ peak from the much stronger Rh—Rh peak with side lobe a modified analysis method had to be used, with a Fourier transformation corrected for phase shift and backscattering amplitude. In this way the side lobe at the low-*R* side of the Rh—Rh peak in the radial structure function, which is caused by the nonlinear *k* dependence of the phase shift and the low-frequency variation in the backscattering amplitude, was removed and the $Rh^0—O^{2-}$ peak became detectable. By subtracting the calculated Rh—Rh contribution to the EXAFS spectrum a difference EXAFS spectrum was obtained, which on forward and backward Fourier transformation proved to be due to a Rh—O distance of 2.7 Å. This distance is much larger than that of $Rh^{3+}—O^{2-}$ in Rh_2O_3 (2.05 Å) and must be due to a $Rh^0—O^{2-}$ distance and not to a $Rh^{3+}—O^{2-}$ distance.

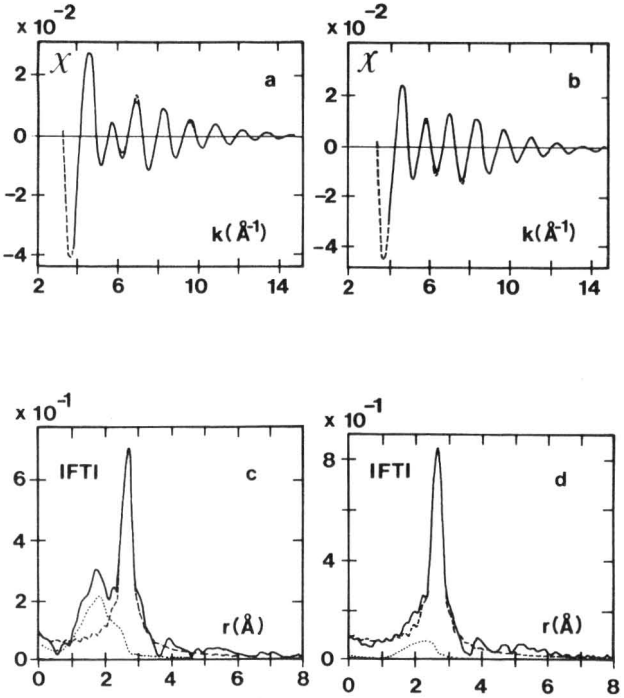

Figure 8.12. EXAFS obtained by back transformation of the Fourier transform of the experimental data (solid line) and the calculated Rh—Rh + Rh—O EXAFS: (*a*) T_{red} = 473 K and (*b*) T_{red} = 673 K. The (k^1) Fourier transform (corrected for the Rh—Rh phase shift and backscattering amplitude) of the experimental data is represented by a solid line. The corresponding Fourier transform of the calculated Rh—Rh EXAFS is given by a dashed curve; the Fourier transform of the calculated Rh—O contribution is indicated by the dotted curve: (*c*) T_{red} = 473 K and (*d*) T_{red} = 673 K. (75).

This proves that indeed structural information is obtained on interfacial rhodium atoms and that the Rh—Al_2O_3 interface apparently consists of rhodium atoms "resting" on O^{2-} anions of the support.

Also the analysis of the rhodium *K*-EXAFS of two Rh/TiO_2 catalysts with H/Rh values of 1.5 and 1.8 showed the presence of long (2.7 Å) Rh^0—O^{2-} distances, besides the Rh—Rh distance (69). Just as in the series of Rh/Al_2O_3 catalysts (77, 78), the measured number of oxygen neighbors for this Rh^0—O^{2-} bond increases with decreasing coordination number of the Rh—Rh bond. For three-dimensional particles the fraction of metal atoms present in the metal-support interface increases with decreasing particle size. This means that both on Al_2O_3 and TiO_2 the rhodium metal particles are three-dimensional rather than two-dimensional one atom thick rafts, because in that case the support oxygen coordination number should have been independent of particle size.

The results for rhodium catalysts were confirmed by a study of a highly dispersed Pt/Al_2O_3 catalyst with $H/Pt = 1.14$ (76). This catalyst [prepared via wet impregnation with $Pt(NH_3)_4(OH)_2$, drying, calcining in flowing O_2 at 623 K, and reduction at 623 K for 2 h] showed after subtraction of the Pt—Pt EXAFS and Fourier transformation of the difference EXAFS signal two peaks in the Fourier transform at 2.05 and 2.65 Å. The first peak must be due to $Pt^{4+}—O^{2-}$ in unreduced PtO_2 particles or Pt^{4+} ions on the support, and the second to $Pt^0—O^{2-}$ in the interface of metallic platinum particles.

All these results demonstrate that interfacial $M^0—O^{2-}$ distance can only reliably be observed if the metal particle size is very small and a high percentage of the metal atoms is located at the interface with the support. The metal–metal coordination number has to be smaller than seven (diameter of the metal particle smaller than 12 Å, if a half-spherical shape is assumed) in order to be able to observe $M^0—O^{2-}$ bonds, because of the weak backscattering property of the (light element) oxygen. In other words one only has a chance of observing these bonds if H/M is close to 1.0.

The EXAFS results show that these well reduced and highly dispersed rhodium and platinum catalysts (in all cases $H/M > 1$) have only $M^0—O^{2-}$ bonds in the metal–support interface. At first sight this may seem surprising because even though the catalysts had been reduced for some time at 673 K their metal particle sizes were very small. One thus might have expected strong ionic interaction forces to be present. Indeed van der Waals forces (induced dipole–induced dipole) will never be able to explain this resistance against sintering. But ion-induced dipole interactions between interfacial O^{2-} anions and rhodium atoms are one or two orders of magnitude stronger and are of the right order of magnitude to explain the adherence of small metal particles to the support.

A supposedly special type of metal–support interaction has attracted quite some attention. This so-called strong metal–support interaction (SMSI) has been invoked to explain the fact that dihydrogen and carbon monoxide can no longer be adsorbed on a noble metal catalyst supported on carriers like TiO_2, when the catalyst is reduced at elevated temperatures ($T > 673$ K). Although at present the SMSI effect is explained by covering of the metal particles by reduced support species than by a special metal–support interaction, the name and acronym still stand (79–81). EXAFS of well-dispersed Pt/TiO_2 catalysts has been measured by Short et al. (82). Their analysis indeed showed small platinum particles to be present with $N_{Pt-Pt} \approx 6$, $R_{Pt-Pt} = 2.70$ Å (somewhat smaller than bulk platinum) and rather large Debye–Waller factors. No Pt—Ti distance could be detected. On the other hand even when such distances would have been present they would have been difficult to discern using the standard method of analysis. New measurements and application of the new data analysis procedure, including the difference file technique and the phase and backscattering

amplitude corrected Fourier transforms, might show interfacial Pt—Ti or Pt—O distances.

8.4.2. Bimetallic Catalysts

Ever since their first introduction in the catalytic reforming process for the manufacture of high octane gasoline, bimetallic catalysts have enjoyed large attention. Present day industrial catalysts therefore usually consist of platinum and a second metal component (iridium, rhenium, tin, or germanium) supported on Al_2O_3. In spite of many investigations the oxidation state of the second component and the structure of the bimetallic catalysts is still under debate. For the Pt—Ir system the opinions diverge least and there is more or less general agreement that both platinum and iridium are fully reduced and intimately mixed in the form of very small alloy particles. Sinfelt calls such particles bimetallic clusters to allow for the possibility of nonideal homogeneity, such as surface enrichment or phase segregation (83). In this chapter we shall adopt the word bimetallic, but we prefer the word particle instead of cluster to denote an aggregate of metal atoms, because the word cluster is already in use in modern inorganic chemistry to denote an aggregate consisting of one or several metal atoms surrounded by organic and or inorganic ligands. For the widely used Pt—Re, Pt—Sn, and Pt—Ge catalysts opinions range, however, from real bimetallic systems— in which both components are in the metallic state and intimately mixed—to systems in which only platinum is metallic and the other component is in the oxidic state (rhenium, tin, or germanium) and not in contact with the platinum particles. Because of these unsolved problems and because of the obvious industrial interest much attention is paid to the characterization of bimetallic catalysts.

Short et al. studied $Pt—Re/Al_2O_3$ (84). Although this study was hampered by noise and many glitches the rhenium L_3-white line intensity was found to be about a factor of two larger than that of the rhenium metal reference powder. Therefore, it was concluded that the majority of the rhenium was present in an oxidic form, probably as Re^{4+}. In agreement with this conclusion the rhenium L_3-EXAFS spectrum showed a peak at $R = 1.95$ Å (corrected for a phase shift of 0.35 Å, close to the value of 0.34 observed in PtO_2). This distance is too short to be explained by metallic Re—Re or Re—Pt distances (about 2.6 Å) and is close to the value of 1.80 Å for the Re—O distance in ReO_2. The conclusion of this study, that rhenium in a $Pt—Re/Al_2O_3$ catalyst is not completely reduced to the metallic state, agrees with that of some catalytic studies, but is in contradication with several other studies (85). This is not too disturbing, however, since it is known, that the reducibility of supported rhenium oxide is

delicately dependent on variables such as water vapor pressure and chlorine content of the catalyst.

Sinfelt, the inventor of the industrial Pt—Ir catalyst that has been put into practice by Exxon, has published the majority of EXAFS studies on bimetallic systems together with Via and Lytle. So far, they have published detailed EXAFS studies on Ru—Cu, Os—Cu, Rh—Cu, Pt—Ir, and Rh—Ir, most of them supported on SiO_2 as well as on Al_2O_3 (86–90). In these articles they not only very carefully addressed the much more abundant problems in the analysis of bimetallic versus monometallic catalysts, but at the same time they obtained a wealth of quantitative information that greatly enlarges our knowledge of such complicated systems. In the following we shall successively discuss their method of analysis and their results.

The analysis of EXAFS data of multicomponent systems is much more complicated than that of one-component systems because the contributions of several EXAFS functions with several different scatterer atoms must be unraveled. A short look at a two-component system (such as a bimetallic catalyst, without taking into consideration the contribution of support atoms) demonstrates the rapidly increasing complexity of the analysis. If we consider the EXAFS function associated with absorber atom X and first-shell neighboring scatterer atoms X and Y, the following equation is obtained:

$$[\chi(k)]_x = [\chi^1(k)]_{xx} + [\chi^1(k)]_{xy} \tag{1}$$

with

$$[\chi^1(k)]_{xy} = [A(k)]_{xy} \sin [\Delta(k)]_{xy} \tag{2}$$

and $A(k)$ and $\Delta(k) = 2kR + \delta(k)$ as defined in Chapter 6, Section 6.3.3.1. An analogous formula can be written down for $[\chi(k)]_y$. Instead of having to determine five parameters from one experimental $\chi(k)$ function in a range of k values for a one-component system, for a two-component system one must determine 18 parameters from two experimental EXAFS functions measured at the x-ray absorption edges of components X and Y. Since the backscattering amplitude is independent of the absorber atom and because of the additivity of the absorber and scatterer contributions to the phase factor (91, 92) the number of parameters is decreased by three. Like in the case of a one-component system, it is almost impossible to disentangle all 15 parameters at once and one therefore uses information on $[F(k)]_x \exp(-2k^2\sigma_{xx}^2)$, $[F(k)]_y \exp(-2k^2\sigma_{yy}^2)$, $[\delta(k)]_{xx}$, $[\delta(k)]_{yy}$, and $[\delta(k)]_{xy}$ from reference materials to extract the following 10 parameters from the two experimental EXAFS functions: N_{xx}, N_{xy}, N_{yx}, N_{yy}, R_{xx}, R_{xy}, R_{yy}, $\Delta\sigma_{xx}^2$, $\Delta\sigma_{xy}^2$, and $\Delta\sigma_{yy}^2$

It is clear that $[F(k)]_x$ and $[F(k)]_y$, in combination with, respectively σ_{xx}^2 and σ_{yy}^2, as well as δ_{xx} and δ_{yy} can be obtained from pure X and Y materials or

from supported monometallic X and Y catalysts. Sinfelt et al. have given two answers to the problem of the determination of δ_{xy}. In their study of RuCu catalysts (86) they have made use of the additivity and transferability of absorber and scatterer contributions to the phase function. By measuring the EXAFS functions of the RuO_2 and Cu_2O metal oxides and of ruthenium and copper metal the phase functions for RuCu and CuRu can be determined:

$$\delta_{RuCu} = \delta_{RuO} + \delta_{CuCu} - \delta_{CuO} \tag{3}$$

$$\delta_{CuRu} = \delta_{CuO} + \delta_{RuRu} - \delta_{RuO} \tag{4}$$

In their paper on Os—Cu Sinfelt et al. (87) introduced another method of determining δ_{xy}. They start with the calculation of a trial function δ_{xy} by using results of theoretical calculations by Teo and Lee (91) of the contributions of absorber and scatterer atoms to the phase shift. Then the phase shift δ_{xy} is altered by varying the threshold absorption energy E_0. In this way a series of trial functions $[\delta(k)]_{xy}$ is obtained, each of which corresponds to a different E_0. By making use of the additivity of the absorber and scatterer contributions to the phase factor the corresponding series of trial functions for $[\delta(k)]_{yx}$ can be calculated. For each set of trial phase functions for xy and yx an iterative least squares analysis is carried out for the two EXAFS functions $[\chi(k)]_x$ and $[\chi(k)]_y$. Thus for each value of E_0 12 N, R, and δ parameters are obtained, including R_{xy} and R_{yx}. In general, R_{xy} will turn out to be inequal to R_{yx}. Therefore, the additional physical constraint that R_{xy} should be equal to R_{yx} is introduced. For Os—Cu and Ir—Rh this led to a single solution for E_0, while for Rh—Cu values of E_0 between -10 and -4 eV were found acceptable. A somewhat unpleasant side effect was that the minimum in the least squares derivation plot was shallow and did not occur at the same value of E_0, which corresponds to the most reasonable physical situation at which $R_{xy} = R_{yx}$.

An alternative method would be to make use of the fact that the parameters $[\Delta(k)]_{xy}$ and $[\Delta(k)]_{yx}$ can both be obtained from the experimental $[\chi(k)]_x$ and $[\chi(k)]_y$ if the $[\chi(k)]_{xx}$ and $[\chi(k)]_{yy}$ contributions could be separated. Since $R_{xy} = R_{yx}$, subtraction of Δ_{yx} from Δ_{xy} gives

$$[\Delta(k)]_{xy} - [\Delta(k)]_{yx} = [\delta(k)]_{xy} - [\delta(k)]_{yx} \tag{5}$$

Because

$$[\delta(k)]_{xy} + [\delta(k)]_{yx} = [\delta(k)]_{xx} + [\delta(k)]_{yy} \tag{6}$$

both sum and difference of $[\delta(k)]_{xy}$ and $[\delta(k)]_{yx}$ are known. Consequently, both phase functions can be obtained and in turn R_{xy} as well. The advantage of

this method is that, in contrast to the other methods, it does not require additional experimental or theoretical information and makes full use of all the information inherent in the EXAFS functions χ_x and χ_y.

The analysis of the Pt—Ir system proved to be even more complicated than the general type of analysis described previously (88). Besides the problem of separating the contributions of platinum and iridium scatterer atoms, which is practically impossible because of the small difference in amplitude and phase functions, there is the additional complication that the iridium and platinum L_3-edges are only 348.5-eV apart, which causes an overlap of the iridium EXAFS function on the platinum EXAFS function. Sinfelt et al. presented a solution to this problem and the related difference in zero point for k. Furthermore, because of the similarity in amplitude and phase functions of platinum and iridium, they combined the two phase terms in χ_{Pt}, as well as in χ_{Ir} by one term only. Such a combination is, however, only allowed if the additional assumption is made that the difference between the PtPt and PtIr interatomic distances, as well as that between those of IrIr and IrPt, is negligible. Although $\Delta_{PtIr} - \Delta_{PtPt} = 2k\Delta R$ is certainly very small compared to Δ_{PtPt} ($R_{PtPt} = 2.775$ Å and $R_{IrIr} = 2.714$ Å), $\Delta_{PtIr} - \Delta_{PtPt}$ is not small compared to one at all, and at high-k values (e.g., above 10 $Å^{-1}$) an interference effect between the sin (Δ_{PtPt}) and sin (Δ_{PtIr}) terms should make itself noticeable. The consequence of using only one phase term in χ_{Pt} and χ_{Ir} is that $R_{PtIr} = R_{PtPt}$ and that $R_{IrPt} = R_{IrIr}$. The least squares procedure then leads to a minimum fitting error for certain values of R_{PtPt} and R_{IrIr}, which in general will be unequal. Indeed Sinfelt et al. found in all three PtIr catalysts differences in R_{PtPt} and R_{IrIr}, which were well beyond the estimated uncertainties. This is, however, physically impossible, since R_{PtIr} has to be equal to R_{IrPt} and thus in their method of analysis all R_{PtPt} and R_{IrIr} distances should have been equal. Only for the PtIr alloy the difference between R_{PtPt} and R_{IrIr} was found to be smaller than the uncertainty of the method. The authors stated that equal distances are to be expected for a completely homogeneous alloy. But this is a (microscopic) misinterpretation of the (macroscopic) rule of Vegard. Although Vegard's rule states that there is a linear relationship between interatomic distance and alloy composition, this does not mean that for every alloy composition all interatomic distances are equal. On the contrary, in principle the interatomic distances R_{xx}, R_{yy}, and $R_{xy} = R_{yx}$ will be different.

Convincing evidence for the deviation from the virtual crystal approximation has been presented by Boyce and Mikkelsen (93, 94) for the ternary systems $Ga_{1-x}In_xAs$, $ZnSe_{1-x}Te_x$, $K_{1-x}Rb_xBr$, and $RbBr_{1-x}I_x$. They demonstrated that first neighbor distances remain closer to the corresponding distances found in the pure binary compounds than to the average (virtual) crystal distance determined from the lattice constant of the ternary phase. Second neighbor distances on the other hand follow Vegard's rule rather well. In view of the fact that the compressibility of Group VIII metals is even smaller than those of the covalent

and ionic compounds studied by Boyce we certainly expect deviations from the virtual crystal approximation for alloys of Group VIII metals.

In view of all this we conclude that some conclusions of the work of Sinfelt et al. will have to be reinvestigated. Thus the statement (87) that a difference in R_{PtPt} and R_{IrIr} indicates that the average composition of the first coordination shell of atoms around platinum is different from that around iridium and the conclusion that in supported Pt—Ir particles there are platinum-rich and iridium-rich regions are premature, at least when based on the results of this EXAFS analysis.

Having discussed the method of analysis of bimetallic particles let us now turn to the results obtained by Sinfelt et al. (86–90). These are tabulated in Table 8.2. The results for Ru—Cu, Os—Cu, and Rh—Cu substantiate the qualitative picture that previous chemisorption and catalytic studies had produced. In these systems, in which the components are immiscible or only slightly miscible (Rh—Cu) in bulk, the bimetallic particles on the support consist of a

Table 8.2. Structural Parameters of Bimetallic Particles Supported on SiO_2 Derived from the EXAFS Data on Both X-Ray Absorption Edges

Metals	Coordination Numbers	Composition First Coordination Shell	Nearest-Neighbor Distances (Å)[b]
RuCu	Ru 11	RuRu 0.92	RuRu 2.65
1:1	Cu 9	CuCu 0.50	CuCu 2.58
			RuCu 2.60
OsCu	Os 12.5	OsOs 0.83	OsOs 2.68
1:1	Cu 9.5	CuCu 0.49	CuCu 2.55
			OsCu 2.68
RhCu		RhRh 0.79	RhRh 2.68
1:1		CuCu 0.50	CuCu 2.62
			RhCu 2.64
RhCu		RhRh 0.92	RhRh 2.68
2:1		CuCu 0.44	CuCu 2.63
			RhCu 2.64
IrRh	Ir 11	IrIr 0.73	IrIr 2.72
1:1	Rh 10	RhRh 0.40	RhRh 2.72
			IrRh 2.72
IrRh[a]	Ir 7	IrIr 0.57	IrIr 2.75
1:1	Rh 5	RhRh 0.60	RhRh 2.71
			IrRh 2.71

[a] Carrier was Al_2O_3.

[b] Nearest-neighbor metal-metal distances in reference monometallic catalysts and metal foils were (Å): Ru/SiO_2, 2.66; Ru, 2.675; Cu/SiO_2, 2.56; Cu, 2.556; Os/SiO_2, 2.70; Os, 2.705; Rh, 2.690; Ir/SiO_2, 2.71; Ir/Al_2O_3, 2.70; Ir, 2.714.

core of ruthenium, osmium or rhodium covered by a layer of copper. Thus the average coordination number of copper is lower than that of the other metal component and the composition of the first coordination shell demonstrates that regions rich in ruthenium, osmium or rhodium exist (Table 8.2). In agreement with the higher miscibility for Rh—Cu it is found that rhodium exhibits a greater tendency than ruthenium or osmium to be coordinated by copper atoms. The Rh—Cu particles presumably contain some copper atoms in the interior of the particles. The fact that the CuCu interatomic distance in Rh—Cu is substantially larger than in metallic Cu—and also larger than in the Ru—Cu and Os—Cu catalyst particles—might also be taken as evidence for the tendency of copper to be present in the interior of the Rh—Cu particles.

In agreement with these results chemisorption of oxygen on a $Ru—Cu/SiO_2$ catalysts changed the copper *K*-EXAFS, but did not change the ruthenium *K*-EXAFS. As can clearly be seen in Fig. 8.13, the magnitude of the ruthenium *K*-EXAFS is decreased upon exposure of dioxygen to a Ru/SiO_2 catalyst (note the difference in left-hand and right-hand scales), but this was not the case for the $Cu—Ru/SiO_2$ catalyst. On the other hand, the magnitude of the copper *K*-EXAFS of Cu/SiO_2 as well as that of the $Cu—Ru/SiO_2$ decreased upon exposure to oxygen and the copper *K*-EXAFS spectrum of $Cu—Ru/SiO_2$ changed dramatically. Thus, the presence of copper in the exterior of bimetallic particles in the $Cu—Ru/SiO_2$ catalyst shields the ruthenium from the oxygen, and only copper is oxidized upon exposure of the $Cu—Ru/SiO_2$ catalyst to oxygen.

Also the Ir—Rh and Pt—Ir systems demonstrated a tendency for segregation and surface enrichment, although the metal components are completely miscible in the bulk. Nevertheless, quite a substantial enrichment of the core of these particles with iridium and of the surface with rhodium and platinum, respectively, was observed. This must be due to the much lower surface tension of rhodium and platinum than of iridium.

A full analysis of interatomic distances and Debye–Waller factors for the bimetallic particles must await further information. The only clear trend is a decrease of the R_{xx} distance and an increase of the R_{yy} distance, when the R_{xx} distance is larger than the R_{yy} distance in the pure metals or monometallic catalysts. Within the uncertainty of the measurements no more information can be obtained for the R_{xy} values than that they are about equal to $\frac{1}{2}(R_{xx} + R_{yy})$. All Debye–Waller factors are much larger than those of the bulk metals and are about as large as those of the monometallic catalyst systems. The uncertainties in σ_1^2 are large, however.

8.4.3. White Lines

Correlations between chemical and electronic properties have always been very popular among chemists and in catalysis especially the relationship between

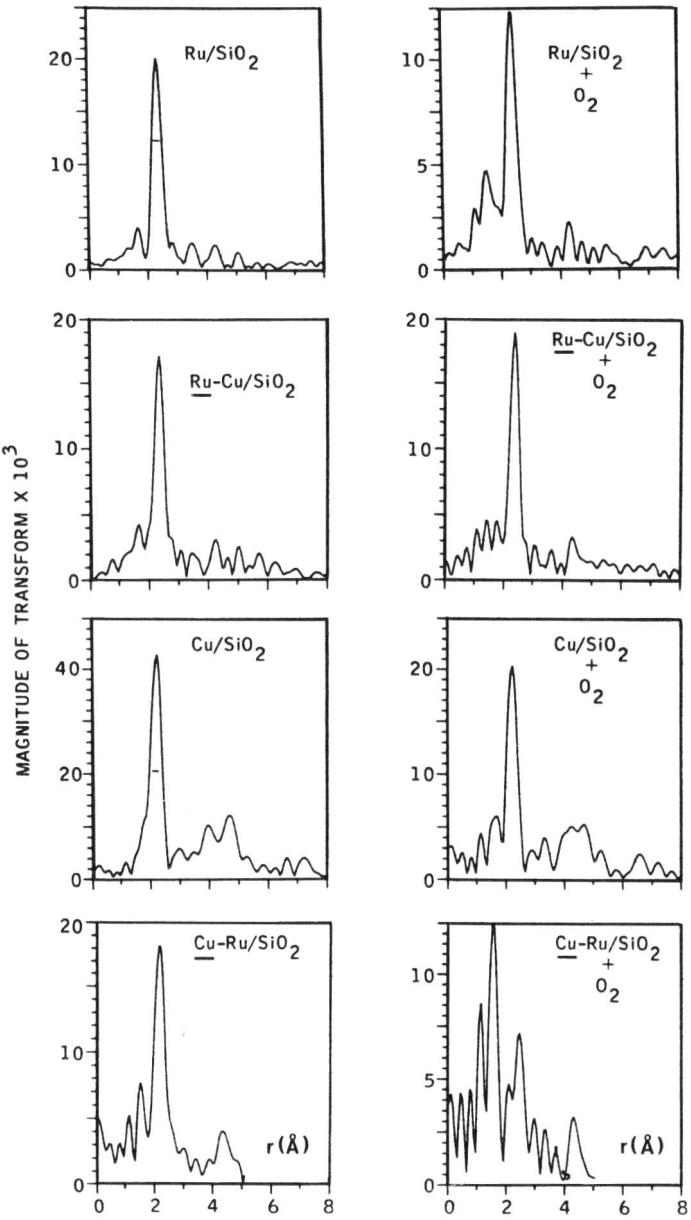

Figure 8.13. Fourier transform (magnitude) of Ru/SiO_2, Cu/SiO_2, and $Cu-Ru/SiO_2$ catalysts before (left-hand side) and after (right-hand side) exposure to oxygen. The metal atom for which the *K*-EXAFS was measured in the bimetallic catalysts is underlined. (86).

catalytic activity and *d*-band character of metal catalysts has been a challenge. It is therefore understandable that the possibility to obtain the *d*-band character directly from the white lines in the x-ray absorption edge structure has attracted much attention. These white lines are due to spectroscopic transitions from $1s$ to p states (K-edge) or $2p$ to d states (L_2 and L_3-edges). Already two decades ago Lewis pointed out the usefulness of x-ray absorption edges for the characterization of metal catalysts (95), but it was only in recent years that interest in this spectroscopic tool really grew. Thus Lytle et al. reported a study of L white lines of metallic gold, platinum, and iridium and of a variety of compounds (6, 96). Compounds had stronger white lines than metals and the intensities could be related to the Pauling ionicity of the metal–ligand bonds in the compounds. They also observed that supported metal catalysts had somewhat more intense white lines than bulk metals, while gas adsorption influenced intensity and shape of the lines (Fig. 8.14). From the fact that platinum (6) and palladium (97) exhibit white lines, but gold (6) and silver (97) do not, it must be concluded that the L white lines are mainly due to $2p$–nd transitions and that the $2p$–$(n + 1)s$ transitions are very weak. This is in accordance with the localized character of the d states and the expanded character of the s states, which do not fit with the $2p$ core hole state.

The observations by Lytle et al. (6) and similar ones by Gallezot et al. (98–100) suggested the possibility that the charge on metal atoms in metal catalysts could be obtained from white line intensities. Since then a number of studies of metal catalysts have been carried out. Because of their close relationship with EXAFS studies on the same catalysts these white line studies will be discussed here. For a more general discussion of white lines and absorption edge structure we refer to Chapter 11.

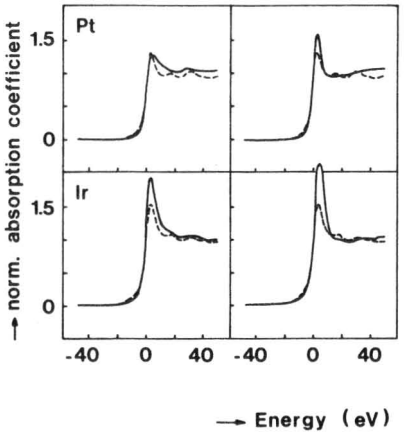

Figure 8.14. L_3-absorption edge spectra of 1 wt.% Pt/Al_2O_3 and 1 wt.% Ir/Al_2O_3 before (left) and after (right) exposure to oxygen, compared with the pure metals (dotted lines) (6).

In all cases studied, for example, platinum on SiO_2 (101), Al_2O_3 (6,101), TiO_2 (82), and Y-zeolite (98), the intensities of the *L* white lines were larger than those of bulk metal. Sintering, gas adsorption, reduction at low and high temperature (82,101) (because of the strong metal support interaction effect in TiO_2), and of alloying (Os—Cu) had noticeable influences on the intensities. These results have in all cases been explained as being due to an increase or a decrease in the number of holes in the 5*d* metal bands and interpreted as demonstrating increases or decreases in the electron deficiencies of supported metal particles relative to bulk metals. Thus it was concluded that small metal particles on supports are slightly electron deficient, that this deficiency is less for platinum particles on TiO_2 than on SiO_2 (82) and that osmium in $Os—Cu/SiO_2$ is less electron deficient than in Os/SiO_2 (87).

This interpretation of *d* vacancies being equal to electron vacancies has important consequences. It does not, however, take into account the possibility that an electron deficiency is not present at all, but that the number of *d* vacancies is just about made up by an increase in the number of *s* electrons via *s*–*d* rehybridization. It is well known that the electronic structure of bulk metal atoms and of isolated metal atoms is different. In general metal atoms have more *d* character in bulk metal, for example, platinum has the configuration $5d^9 6s^1$ in atoms and $5d^{9.7} 6s^{0.3}$ in bulk metal. Because of this one might expect that metal atoms with intermediate geometry, like in crystal surfaces or in small metal particles, have an intermediate electronic structure. Metal atoms with an incomplete shell of neighbors will have smaller local *d* and *s* bandwidths and thus have electronic structures intermediate between those of isolated atoms and fully surrounded atoms in bulk metal. All this means that a change in the metal particle size is very likely to be accompanied by a change in the state of hybridization of the metal atoms involved (102, 103).

Several theoretical calculations have demonstrated that the rehybridization model is correct (104). Also photoemission experiments have confirmed this (102). It therefore seems logical to try and explain the experimental white line results of metal catalysts by rehybridization instead of electron deficiency. Indeed all results obtained so far can be explained by rehybridization due to changes in particle size. Thus the fact that the intensity of the white lines of Pt/TiO_2 is intermediate between those of bulk platinum and Pt/SiO_2 (82) agrees with the better dispersion of platinum on SiO_2. The fact that the intensity for $Os—Cu/SiO_2$ is smaller than that of Os/SiO_2 but larger than that of bulk osmium (87) (Fig. 8.15), demonstrates again that in $Os—Cu/SiO_2$ the copper is present as an outer layer on the osmium particles. As a result the osmium atoms will on the average have more neighboring metal atoms than the osmium atoms in Os/SiO_2. Furthermore, the outcome of the study of Short et al. (82) on Pt/TiO_2 might need modification, although their conclusion that the platinum atoms on TiO_2 are slightly less electron deficient than those on SiO_2 or Al_2O_3

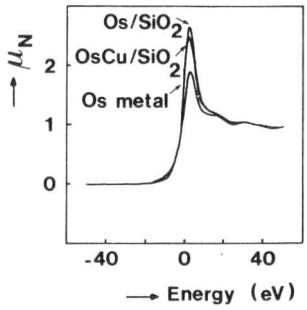

Figure 8.15. L_3-absorption edge spectra of bulk Os, Os/SiO_2, and $Os-Cu/SiO_2$ catalysts (87).

was already a disappointment to believers in the charge transfer explanation for the SMSI effect. The observation that the white line intensity of Pt/TiO_2 reduced at high temperature is smaller than that of the same catalysts reduced at low temperature, and that this intensity in turn is smaller than that of Pt/SiO_2, then just means that the *d*-electron deficiency increases in this order because of decreasing platinum particle size. Because of *s*–*d* rehybridization this does not (have to) mean that the total number of electrons on platinum also decreases in this order. Indeed the Pt/TiO_2 catalysts appear to have a slightly higher first-shell coordination number after high temperature reduction (82).

The question of the white line intensities is certainly not solved, but for the moment there is every reason to doubt the explanation in terms of electron deficiency. Another question that remains to be solved is the fact that not only changes in L_3 intensity have been observed, but also of L_2 intensity (82, 101, 105). This is surprising since the L_2 $2p_{1/2} - 5d_{3/2}$ transition is expected to be much weaker than the L_3 $2p_{3/2} - 5d_{3/2}$, $5d_{5/2}$ transitions, because of the fact that the large spin-orbit splitting of the platinum $5d$ band makes the holes go predominantly to the $j = \frac{5}{2}$ state (106, 107). In accordance with this the L_2-edge of bulk platinum hardly shows a white line. But if a platinum atom is situated in a position of much lower symmetry than spherical, such as at the metal surface or metal–support interface, then mixing of the *d* bands might occur and the L_2 band might "steal" intensity from the L_3 white line.

The formation of the core hole in the absorbing atom strongly perturbs the potential of that atom and as a result in insulators the excited states, which are localized on the perturbed atom, may be pulled down in energy below the conduction band. In that case a cluster approximation will better describe the experimental results than a delocalized band model. Therefore, Kutzler et al. (108) and Horsley (105) carried out $X\alpha$ molecular orbital cluster calculations of the absorption cross sections of *K*-edge transitions for some transition metal compounds. The calculations were rather successful in reproducing the experi-

mental features. Even so, more theoretical studies are needed to increase our knowledge about near-edge structure. Especially calculations on relaxation effects in metals after the excitation of a core electron to an excited state would be of interest. Horsley performed such a calculation in the local cluster approximation (105). Interest in x-ray absorption edge spectroscopy is indeed growing in catalysis, as for instance exemplified by the study of Sham (109). By combining spin-orbit coupling with ligand field theory he was able to explain the occurrence of specific white lines in the *L*-edges of $Ru(NH_3)_6Cl_3$. Many more examples of edge structures are presented and discussed in Chapter 11, Sections 11.5.8, 11.5.9, and 11.7.4.

8.5. CONCLUSIONS

Even though EXAFS is a young technique already quite a few very important results have been obtained in catalysis. Especially the results on Wilkinson's catalyst (Section 8.3.1), the sulfided $Co-Mo/Al_2O_3$ catalyst (Section 8.3.3), bromine and krypton on graphite (Section 8.3.4), and the mono and bimetallic catalysts (Sections 8.4.1 and 8.4.2) are worth mentioning. In homogeneous catalysis the results have much in common with those reported on metal containing enzymes in biochemistry and *in situ* EXAFS studies allow a detailed picture to be obtained of the environment of the metal atom. In heterogeneous catalysis the best studies published so far have provided information of about the same quality as that obtained by the SEXAFS technique on adsorbates on single crystal surfaces. Therefore, it is expected that studies on highly dispersed catalysts will aid in developing a detailed picture of catalyst support interfaces and of the interaction playing a role in the bonding of catalyst particles to the support. Great difficulties will lay ahead, though, because the normal EXAFS technique is a bulk technique and thus not only metal atoms in the interface between metal particle and support will be measured but also all other metal atoms on top of those in the interface. Furthermore, the support oxygen ions have a low backscattering amplitude. For these reasons especially catalysts with very high dispersions are of interest. Such catalysts can in general only be prepared at low metal loading, which brings us to the problem of signal-to-noise ratio. Therefore, the trend in the applications of EXAFS in catalysis in the coming years will undoubtedly be to try for lower and lower catalyst loadings, which experimentally means that one ultimately has to switch from normal transmission detection to fluorescence detection.

Another area of interest for EXAFS in catalysis will be the morphology of catalyst particles with such a small size that they are not measurable with a

technique like x-ray diffraction. For such small particles ($d < 3$ nm) electron microscopy also fails to be of help since if it is not used under *in situ* conditions it will only provide information of the catalyst in the passivated state. For such small particles this state is not much different from the completely oxidized state. Also, in this application of EXAFS the S/N ratio will be a problem to overcome, because the study by Greegor and Lytle (49) has already shown that unambiguous information on particle shape and size can only be inferred if good data are available on the higher coordination shells too.

The comming years will show the ultimate position of the EXAFS technique in catalysis. Like biochemistry, catalysis has been and undoubtedly will be a field in which multidisciplinary approaches are welcome and in which many techniques have found application. Of course EXAFS cannot, and has never claimed to be able to solve every problem, but in combination with other physical and chemical approaches it will certainly have a great impact on catalysis.

REFERENCES

1. S. Wanke and N. A. Dougharty, *J. Catal.*, **24,** 367 (1972).
2. R. W. Joyner, J. A. R. van Veen, and W. M. H. Sachtler, *J. Chem. Soc. Faraday Trans. I*, **78,** 1021 (1982).
3. J. Reed, P. Eisenberger, and J. Hastings, *Inorg. Chem.*, **17,** 481 (1978).
4. G. Vlaic, J. C. J. Bart, W. Cavigiolo, S. Mobilio, and G. Navarra, *Chem. Phys.*, **64,** 115 (1982).
5. R. M. Friedman, J. F. Freeman, and F. W. Lytle, *J. Catal.*, **55,** 10 (1978).
6. F. W. Lytle, P. S. P. Wei, R. B. Greegor, G. H. Via, and J. H. Sinfelt, *J. Chem. Phys.*, **70,** 4849 (1979).
7. F. W. Lytle, R. B. Greegor, E. C. Marques, D. R. Sandstrom, G. H. Via, and J. H. Sinfelt, in *Proceedings of the Advances in Catalytic Chemistry II*, Salt Lake City, May 1982.
8. E. A. Stern and S. Heald, *Rev. Sci. Instrum.*, **50,** 1579 (1979).
9. J. M. Lorntson, Ph.D. dissertation, University of Delaware, Newark, 1980.
10. B. S. Clausen, B. Lengeler, R. Candia, J. Als-Nielsen, and H. Topsøe, *Bull. Soc. Chim. Belg.*, **90,** 1249 (1981).
11. M. Boudart, R. Dalla Betta, K. Foger, and D. G. Löffler, in *EXAFS and Near Edge Structure III*, K. O. Hodgson, B. Hedman, and J. E. Penner-Hahn (Eds.), Springer-Verlag, Berlin, 1984, p. 187.
12. D. C. Koningsberger and J. W. Cook Jr., in *EXAFS and Near Edge Structure* (*Chemical Physics*, Vol. 27), A. Bianconi, L. Incoccia, and S. Stipcich (Eds.), Springer-Verlag, Berlin, 1983, p. 412.
13. J. Reed, P. Eisenberger, B. K. Teo, and B. M. Kincaid, *J. Am. Chem. Soc.*, **99,** 5217 (1977).

14. J. Reed and P. Eisenberger, *J. Chem. Soc. Chem. Commun.*, 628 (1977).
15. J. Reed, P. Eisenberger, B. K. Teo, and B. M. Kincaid, *J. Am. Chem. Soc.*, **100,** 2375 (1978).
16. R. M. Stults, R. M. Friedman, K. Koenig, W. Knowles, R. B. Greegor, and F. W. Lytle, *J. Am. Chem. Soc.*, **103,** 3235 (1981).
17. J. Goulon, E. Georges, C. Goulon-Ginet, Y. Chauvin, D. Commereuc, H. Dexpert, and E. Freund, *Chem. Phys.*, **83,** 357 (1984).
18. B. Besson, B. Moraweck, A. K. Smith, J. M. Basset, R. Psaro, A. Fusi, and R. Ugo, *J. Chem. Soc. Chem. Commun.*, 569 (1980).
19. T. Yokoyama, K. Yamazaki, N. Kosugi, H. Kuroda, M. Ichikawa, and T. Fukushima, *J. Chem. Soc. Chem Commun.*, 962 (1984).
20. F. W. Lytle, D. E. Sayers, and E. B. Moore, Jr., *Appl. Phys. Lett.*, **24,** 45 (1974).
21. R. B. Greegor, F. W. Lytle, R. L. Chin, and D. M. Hercules, *J. Phys. Chem.*, **85,** 1232 (1981).
22. R. Shulman, Y. Yafet, P. Eisenberger, and W. Blumberg, *Proc. Natl. Acad. Sci., USA*, **73,** 1384 (1976).
23. K. Tohji, Y. Udagawa, S. Tanabe, and A. Ueno, *J. Am. Chem. Soc.*, **106,** 612 (1984).
24. K. Tohji, Y. Udagawa, S. Tanabe, T. Ida, and A. Ueno, *J. Am. Chem. Soc.*, **106,** 5172 (1984).
25. R. Kozlowski, R. F. Pettifer, and J. M. Thomas, *J. Chem. Soc. Chem. Commun.*, 438 (1983); and *J. Phys. Chem.*, **87,** 5172, 5176 (1983).
26. G. Vlaic, J. C. J. Bart, W. Cavigiolo, S. Mobilio, and G. Navarra, *Z. Naturforsch.*, **36A,** 1192 (1981).
27. Y. Sato, Y. Iwasawa, and H. Kuroda, *Chem. Lett.*, 1101 (1982).
28. T. I. Morrison, A. H. Reiss, Jr., E. Gebert, L. E. Iton, G. D. Stucky, and S. L. Suib, *J. Chem. Phys.*, **72,** 6276 (1980).
29. T. I. Morrison, L. E. Iton, G. K. Shenoy, G. D. Stucky, S. L. Suib, and A. H. Reiss, Jr., *J. Chem. Phys.*, **73,** 4705 (1980).
30. T. I. Morrison, L. E. Iton, G. K. Shenoy, G. D. Stucky, and S. L. Suib, *J. Chem. Phys.*, **75,** 4086 (1981).
31. B. S. Clausen, H. Topsøe, R. Candia, J. Villadsen, B. Lengeler, J. Als-Nielsen, and F. Christensen, *J. Phys. Chem.*, **85,** 3868 (1981).
32. M. Boudart, J. Sanchez Arrieta, and R. Dalla Betta, *J. Am. Chem. Soc.*, **105,** 6501 (1983).
33. T. G. Parham and R. P. Merrill, *J. Catal.*, **85,** 295 (1984).
34. N. S. Chiu, S. H. Bauer, and M. F. L. Johnson, *J. Catal.*, **89,** 226 (1984).
35. I. Kohatsu, D. W. Blakely, and H. F. Hansberger, in *Synchrotron Radiation Research*, H. Winick and S. Doniach (Eds.), Plenum, New York, 1980, p. 417.
36. B. S. Clausen, H. Topsøe, R. Candia, and B. Lengeler, in *EXAFS and Near Edge*

Structure III, K. O. Hodgson, B. Hedman, and J. E. Penner-Hahn (Eds.), Springer-Verlag, Berlin, 1984, p. 181.

37. P. Grange, *Catal. Rev. Sci. Eng.*, **21,** 135 (1980).
38. P. Eisenberger and G. S. Brown, *Solid State Commun.*, **29,** 481 (1979).
39. G. S. Brown, in *Synchroton Radiation Research*, H. Winick and S. Doniach (Eds.), Plenum, New York, 1980, p. 387.
40. G. Bunker, in *EXAFS and Near Edge Structure III*, K. O. Hodgson, B. Hedman, and J. E. Penner-Hahn (Eds.), Springer-Verlag, Berlin, 1984, p. 268.
41. W. L. Schaich, in *EXAFS and Near Edge Structure III*, K. O. Hodgson, B. Hedman, and J. E. Penner-Hahn (Eds.), Springer-Verlag, Berlin, 1984, p. 2.
42. H. Topsøe, B. S. Clausen, R. Candia, C. Wivel, and S. Mørup, *J. Catal.*, **68,** 433 (1981).
43. E. A. Stern, D. E. Sayers, J. G. Dash, H. Shechter, and B. Bunker, *Phys. Rev. Lett.*, **38,** 767 (1977).
44. S. M. Heald and E. A. Stern, *Phys. Rev. B*, **17,** 4069 (1978).
45. C. Bouldin and E. A. Stern, *Phys. Rev. B*, **25,** 3462 (1982).
46. G. H. Via, J. H. Sinfelt, and F. W. Lytle, *J. Chem. Phys.*, **71,** 690 (1979).
47. J. H. Sinfelt, G. H. Via, and F. W. Lytle, *J. Chem. Phys.*, **68,** 2009 (1978).
48. E. Marques, D. R. Sandstrom, F. W. Lytle, and R. B. Greegor, *J. Chem. Phys.*, **77,** 1027 (1982).
49. R. B. Greegor and F. W. Lytle, *J. Catal.*, **63,** 476 (1980).
50. B. Moraweck, C. Clugnet, and A. J. Renouprez, *Surf. Sci.*, **81,** L 631 (1979).
51. B. Moraweck and A. J. Renouprez, *Surf. Sci.*, **106,** 35 (1981).
52. A. Renouprez, P. Fouilloux, and B. Moraweck, in *Growth and Properties of Metal Clusters*, J. Bourdon (Ed.), Elsevier, Amsterdam, 1980, p. 421.
53. G. Apai, J. F. Hamilton, J. Stöhr, and A. Thompson, *Phys. Rev. Lett.*, **43,** 165 (1979).
54. J. F. van der Veen, F. J. Himpsel, and D. E. Eastman, *Phys. Rev. B*, **25,** 7388 (1982).
55. P. Lagarde, in *EXAFS and Near Edge Structure* (*Chemical Physics*, Vol. 27), A. Bianconi, L. Incoccia, and S. Stipcich (Eds.), Springer-Verlag, Berlin, 1983, pp. 296 and 319.
56. P. Lagarde, T. Murata, G. Vlaic, E. Freund, H. Dexpert, and J. P. Bournonville, *J. Catal.*, **84,** 333 (1983).
57. H. Dexpert, P. Lagarde, and J. P. Bournonville, *J. Mol. Catal.*, **25,** 347 (1984).
58. D. Bazin, H. Dexpert, P. Lagarde, and J. P. Bournonville, in *EXAFS and Near Edge Structure III*, K. O. Hodgson, B. Hedman, and J. E. Penner-Hahn (Eds.), Springer-Verlag, Berlin, 1984, p. 195.
59. R. W. Joyner, *J. Chem. Soc. Faraday Trans. I*, **76,** 357 (1980).
60. R. K. Nandi, F. Molinero, C. Tang, J. B. Cohen, J. B. Butt, and R. L. Burwell, Jr., *J. Catal.*, **78,** 289 (1982).

61. R. K. Nandi, P. Georgeopoulos, J. B. Cohen, J. B. Butt, R. L. Burwell, Jr., and D. H. Bilderback, *J. Catal.*, **77,** 421 (1982).

62. J. C. Vis, H. F. J. van 't Blik, T. Huizinga, J. van Grondelle, and R. Prins, *J. Mol. Catal.*, **25,** 367 (1984).

63. T. Fukushima, J. R. Katzer, D. E. Sayers, and J. W. Cook, Jr., in *Proceedings of the 7th International Congress on Catalysis*, T. Seyama and K. Tanabe (Eds.), Elsevier, Amsterdam, 1981, p. 79.

64. F. W. Lytle, G. H. Via, and J. H. Sinfelt, *J. Chem. Phys.*, **67,** 3831 (1977).

65. A. D. Cox, in *Characterization of Catalysts*, J. M. Thomas and P. Lambert (Eds.), Wiley, London, 1981, p. 254.

66. H. F. J. van 't Blik, J. B. A. D. van Zon, T. Huizinga, J. C. Vis, D. C. Koningsberger, and R. Prins, *J. Phys. Chem.*, **87,** 2264 (1983).

67. H. F. J. van 't Blik, J. B. A. D. van Zon, T. Huizinga, J. C. Vis, D. C. Koningsberger, and R. Prins, *J. Am. Chem. Soc.*, **107,** 3139 (1985).

68. H. F. J. van 't Blik, J. B. A. D. van Zon, D. C. Koningsberger, and R. Prins, *J. Mol. Catal.*, **25,** 379 (1984).

69. D. C. Koningsberger, H. F. J. van 't Blik, J. B. A. D. van Zon, and R. Prins, in *Proceedings of the 8th International Congress on Catalysis*, Verlag Chemie, Weinheim, 1984, p. V-123.

70. D. C. Koningsberger, in *EXAFS and Near Edge Structure III*, K. O. Hodgson, B. Hedman, and J. E. Penner-Hahn (Eds.), Springer-Verlag, Berlin, p. 212.

71. Y. I. Yermakov and B. N. Kuznetsov, *J. Mol. Catal.*, **9,** 13 (1980).

72. E. G. Derouane, A. J. Simoens, and J. C. Vedrine, *Chem. Phys. Lett.*, **52,** 549 (1977).

73. I. W. Bassi, F. Garbassi, G. Vlaic, A. Marzi, G. R. Tauszik, G. Cocco, L. Galvagno, and G. Parravano, *J. Catal.*, **64,** 405 (1980).

74. I. W. Bassi, F. W. Lytle, and G. Parravano, *J. Catal.*, **42,** 139 (1976).

75. D. C. Koningsberger, J. B. A. D. van Zon, H. F. J. van 't Blik, G. J. Visser, R. Prins, A. N. Mansour, D. E. Sayers, D. R. Short, and J. R. Katzer, *J. Phys. Chem.*, **89,** 4075 (1985).

76. D. C. Koningsberger and D. E. Sayers, *Solid State Ionics*, **16,** 23 (1985).

77. J. B. A. D. van Zon, D. C. Koningsberger, H. F. J. van 't Blik, R. Prins, and D. E. Sayers, *J. Chem. Phys.*, **80,** 3914 (1984).

78. J. B. A. D. van Zon, D. C. Koningsberger, H. F. J. van 't Blik, and D. E. Sayers, *J. Chem. Phys.*, **82,** 5742 (1985).

79. S. J. Tauster, S. C. Fung, and R. L. Garten, *J. Am. Chem. Soc.*, **100,** 170 (1978).

80. J. Santos, J. Phillips, and J. A. Dumesic, *J. Catal.*, **81,** 147 (1983).

81. H. F. J. van 't Blik, P. H. A. Vriens, and R. Prins, *Strong Metal-Support Interactions*, in R. T. K. Baker, and S. J. Tauster, J. A. Dumesic (Eds.), ACS Symposium Series 298, American Chemical Society, Washington DC, 1985, p. 60.

82. D. R. Short, A. N. Mansour, J. W. Cook, Jr., D. E. Sayers, and J. R. Katzer, *J. Catal.*, **82,** 299 (1983).

83. J. H. Sinfelt, *Acc. Chem. Res.*, **10,** 15 (1977).
84. D. R. Short, S. M. Khalid, J. R. Katzer, and M. J. Kelley, *J. Catal.*, **72,** 288 (1981).
85. N. Wagstaff and R. Prins, *J. Catal.*, **59,** 434 (1979).
86. J. H. Sinfelt, G. H. Via, and F. W. Lytle, *J. Chem. Phys.*, **72,** 4832 (1980).
87. J. H. Sinfelt, G. H. Via, F. W. Lytle, and R. B. Greegor, *J. Chem. Phys.*, **75,** 5527 (1981).
88. J. H. Sinfelt, G. H. Via, and F. W. Lytle, *J. Chem. Phys.*, **76,** 2779 (1982).
89. G. Meitzner, G. H. Via, F. W. Lytle, and J. H. Sinfelt, *J. Chem. Phys.*, **78,** 882 (1983).
90. G. Meitzner, G. H. Via, F. W. Lytle, and J. H. Sinfelt, *J. Chem. Phys.*, **78,** 2533 (1983).
91. B. K. Teo and P. A. Lee, *J. Am. Chem. Soc.*, **101,** 2815 (1979).
92. P. H. Citrin, P. Eisenberger, and B. M. Kincaid, *Phys. Rev. Lett.*, **36,** 1346 (1976).
93. J. C. Mikkelsen, Jr. and J. B. Boyce, *Phys. Rev. B*, **28,** 7130 (1983).
94. J. B. Boyce and J. C. Mikkelsen, Jr., in *EXAFS and Near Edge Structure III*, K. O. Hodgson, B. Hedman, and J. E. Penner-Hahn (Eds.), Springer-Verlag, Berlin, 1984, p. 426.
95. P. H. Lewis, *J. Phys. Chem.*, **64,** 1103 (1960); **66,** 105 (1962); **67,** 2151 (1963); and *J. Catal.*, **43,** 376 (1968).
96. F. W. Lytle, *J. Catal.*, **43,** 376 (1976).
97. T. K. Sham, *Phys. Rev. B*, **31,** 1888 (1985).
98. P. Gallezot, R. Weber, R. A. Dalla Betta, and M. Boudart, *Z. Naturforsch.*, **34A,** 40 (1979).
99. P. H. Lewis, *J. Catal.*, **69,** 511 (1981).
100. R. A. Dalla Betta, M. Boudart, P. Gallezot, and R. S. Weber, *J. Catal.*, **69,** 514 (1981).
101. A. N. Mansour, J. W. Cook, Jr., D. E. Sayers, R. J. Emrich, and J. R. Katzer, *J. Catal.*, **89,** 462 (1984).
102. M. G. Mason, *Phys. Rev. B*, **27,** 748 (1983).
103. P. H. Citrin and G. K. Wertheim, *Phys. Rev. B*, **27,** 3160 (1983).
104. C. S. Wang and A. J. Freeman, *Phys. Rev. B*, **19,** 793 (1979).
105. J. A. Horsley, *J. Chem. Phys.*, **76,** 1451 (1982).
106. M. Brown, R. E. Peierls, and E. A. Stern, *Phys. Rev. B*, **15,** 738 (1977).
107. L. F. Mattheiss and R. E. Dietz, *Phys. Rev. B*, **22,** 1663 (1980).
108. F. W. Kutzler, C. R. Natoli, D. K. Misemer, S. Doniach, and K. O. Hodgson, *J. Chem. Phys.*, **73,** 3274 (1980).
109. T. K. Sham, *J. Am. Chem. Soc.*, **105,** 2269 (1983).